THIRD QUARTERLY REPORT
24 February through 23 May 1964

on

Use of Optical Masers in Displays and Printers

Technical Requirement SCL-4396, 6 June 1962
Contract No. DA-36-039-AMC-00118 (E)
Order No. 5389-PM-63-91; PR & C No. 63-ELN/R-6505

to

U. S. Army Electronics Research and Development Laboratory
Fort Monmouth, New Jersey

The objective of this study and investigation is a significant improvement in the state of the art among electro-optical input/output devices using the Laser as an electro-optic tool.

Report Prepared by:
Dr. W. Kulcke, Mr. K. Kosanke
Dr. E. Max, Dr. H. Fleisher
Development Laboratory, Data Systems Division
International Business Machines Corporation, Poughkeepsie, New York

CONTENTS

FIGURES

PURPOSE

Speed and storage capabilities of data processing systems have increased steadily in the past decade. The display of results and information produced by computers handling problems of such high speeds must be accomplished by similarly sophisticated approaches.

In addition to the display of hard copy production of alpha-numeric material , we must consider two-dimensional and multidimensional display of graphic and analog type information. The display must be compatible with the human in terms of matching his frequency range of sensitivity, resolving power, and image retention.

The immediate prupose of this study is to develop a model of a digital electro-optic light deflector for directing a convergent light beam to one of 256 x 256 discrete output positions in two dimensions of a screen.

We shall also develop circuitry capable of switching KDP crystals at a 100 kc rate, and indicate guide lines for design of higher speed switching circuits. A high-speed digital light deflector will be the means of applying laser technology to such computer devices as display and high-speed printing.

ABSTRACT

This report is concerned with further investigations into the Digital Electro-Optic Deflector.

Design specifications related to aperture, spot size, spot position and background light (noise) are calculated as functions of the number of deflection stages for various crystal materials.

From the calculations, the specifications of the birefringent and electro-optic crystals and their tolerances were evaluated for a two-dimensional deflector of 256 x 256 positions.

The relation between the address of an output position and the input signal to the switches is reported; and the distribution of noise, i.e. the light intensity in unswitched positions is described. Further investigations refer to the frequency response and the electrode problem of the electro-optic crystals.

Two electronic circuits which appear to be suited for high speed, low power switching of the light deflector are discussed.

NEXT QUARTER PLANS

The mathematical analysis of the influence of fabrication tolerances on the performance of the light deflector will be concluded.

We will receive the electro-optic KD*P crystals and the birefringent calcite crystals to be used in the model of the 256 x 256 position light deflector. These crystals will be checked optically to determine whether they are within tolerances. We will investigate methods of cementing these crystals together in adjusted orientations.

The semitransparent electrodes of the electro-optic crystals will be further investigated. This work comprises the measurement of resistivity and dielectric strength of DPON+DTA cement in various formulations. KDP crystals will be cemented to electrodes and checked at d-c and a-c voltages. The investigations of physical properties of KD*P crystals will be continued. These comprise measurements of resonant frequencies of the crystals under damped and undamped conditions, dielectric losses, and thermal conductivity.

We shall continue our investigation of several approaches to high-speed switching of the KD*P crystals in order to determine the most acceptable circuit.

PUBLICATIONS, LECTURES, REPORTS AND CONFERENCES

Publications

A paper on "A Fast Digital-Indexed Light Deflector" was published in IBM Journal of Research and Development, Vol. 8, No. 1, 1964, by W. Kulcke, T. J. Harris, K. Kosanke, E. Max.

Conferences

On 11 March 1964 Mr. P. Siglin visited the IBM Laboratory Poughkeepsie, N. Y. and checked the bread-board model of the electro-optic light deflector with eight positions, which was the subject of the previous contract. The model was accepted.

A conference was held on 6 April 1964 at IBM Poughkeepsie, N. Y. between Messrs. P. Siglin, W. Huber, E. Kral and Dr. H. Bennet of Ft. Monmouth; Mr. Eugene Manpin of Wright-Patterson Air Force Base; Lt. J. Davis, Messrs J. Tippett and R. Thompson of NSA; and Messrs. H. Fleisher, W. Kulcke, E. Max, K. Kosanke, and T. Harris of IBM Poughkeepsie

Subjects of the conference were new developments of optical and electro-optical technologies and their potential applications to Data Processing Systems.

I. INTRODUCTION

Electronic control of light beams is of significant interest for computer input/output devices such as displays and high-speed printing. Under the previous contract, to which the present contract is an extension, we investigated several approaches for controlling, particularly deflecting, light beams under the influence of electrical signals. The results of that contract are described in four reports [1,2,3,4]. From these investigations, we determined that the digital electro-optic light deflector is the most promising of the various approaches considered. It yields a fast, jitter-free, random positioning of a light beam to any one of a large multitude of different positions. Utilizing a laser as a light source, the output brightness is several orders of magnitude larger than that achievable by phosphors in cathode ray tubes.

These properties were demonstrated by a bread-board model of a three-stage light deflector producing eight linearly arranged positions with a collimated light beam. With the use of this model, we determined the problems to be encountered for building light deflectors with very large numbers of output positions of the light beam.

The purpose of our work under the current contract is to build a model of a digital electro-optic light deflector for convergent beams, capable of deflecting the light into $2^8 \times 2^8$ (256×256) discrete positions along the x and y axes. As a further subject of the contract, electronic circuits are being investigated for switching electro-optic crystals at rates up to 10^5 pulses per second. This work is aimed at building a feasibility model of such an electronic switch.

In pursuing these subjects, we worked in three major fields, the work being described in the following sections of this report. The first field (Secs. 2, 3, 4, and 5) deals with the determination of the specifications and tolerances of the birefringent and electro-optic crystals for digital electro-optic light deflectors. The respective calculations are performed on a general basis. The specifications and tolerances resulting for the projected model are extracted and given in Sec. 6.

For different applications of the deflector, characteristic properties have to be considered. Two essential properties, the code of the output positions and the noise distribution are investigated in the second field. The results are reported in Secs. 7 and 8.

The subject of the third field are problems connected with the switching process of the electro-optic crystals. These are the frequency response of the crystals, the problem of electrodes, and electronic circuits for high speed switching. These problems are discussed in Secs. 9, 10, and 11.

2. ORIENTATION OF THE BIREFRINGENT CRYSTALS

2.1 CALCULATION OF THE MAXIMUM ANGLE OF SPLITTING AND THE CORRESPONDING CUTTING ANGLE

For a properly oriented birefringent crystal, an unpolarized light beam normally incident onto the crystal is split into two rays -- the ordinary and the extraordinary ray. Both rays travel through the crystal in different directions. The splitting angle between these two rays depends on the crystal material, the crystallographic orientation and the wavelength of the light used. In the first quarterly report[1] the splitting angle ϵ was calculated as a function of the cutting angle γ, i.e., the angle between the surface normal and the optic axis of the crystal, for only one material and one wavelength ($CaCO_3$ at $\lambda = 546.1 m\mu$).

In the meantime, two other crystal materials were considered to be important in the design of a light deflector: Sodium nitrate ($NaNO_3$) and Potasium dihydrogen phosphate ($K H_2PO_4$ or KDP). $NaNO_3$ is an artifically grown crystal which has a splitting angle being about 30% larger than the one in calcite. KDP is of interest as a substitute for either calcite or sodium nitrate in the first few stages of a light deflector. In a high-resolution light deflector where a small beam separation is necessary, these crystals would have to be very thin if they would be designed of materials with a large splitting angle. Since the splitting angle of KDP is relatively small, the required thickness is much more practical to work with. Another possibility to increase the thickness and to use the same material throughout the deflector would be to change the cutting angle γ. For small splitting angles, ϵ depends much more on the angle of cutting than in the region of ϵ_{max}. Therefore, small variations in the orientation have a comparatively large influence on the separation of the beams.

For three materials, $CaCO_3$, $NaNO_3$, and KDP, the splitting angle ϵ as a function of the cutting angle γ is shown in figures 2.1 - 2.3. Since the laser is of greater interest as a light source for the deflector than other sources, these calculations were made for $\lambda = 632.8 m\mu$, the wavelength of the He-Ne gas laser.

The maximum splitting angle and the corresponding cutting angle are calculated for the three materials at $\lambda = 632.8 m\mu$ using the equation given in the first quarterly report[1].

$$\epsilon_{max} = -\frac{\pi}{2} + \arcsin\frac{n_e}{\sqrt{n_c^2 + n_o^2}} + \arctan\left(\frac{n_e}{n_o}\right)$$

$$= -\arctan\frac{n_o^2 - n_e^2}{2\, n_o n_e}$$

and

$$\gamma_{max} = \arcsin\frac{n_e}{\sqrt{n_e^2 + n_o^2}}$$

The results of these calculations are:

Crystal Material	ϵ_{max} in degrees	γ_{max} in degrees
$NaNO_3$	9.64	40.18
$CaCO_3$	6.22	41.89
KH_2PO_4	1.56	44.22

2.2 CALCULATION OF THE ISOTROPIC ANGLE OF SPLITTING AND THE CORRESPONDING CUTTING ANGLE

The light deflector, to be built under this contract, is designed for a convergent rather than a parallel light beam. Therefore, the influence of oblique incidence on the splitting angle ϵ was theoretically investigated.

In Figure 2.4 a light beam, LO, is incident under an angle β onto a crystal surface which is cut at an angle γ relative to the optic axis of the crystal material. This beam is split into two components -- the ordinary and the extraordinary. The ordinary component is refracted according to Snell's law. In the extraordinary component, only the wave normal obeys this law whereas the ray vector of the extraordinary beam does not. In the ordinary component, the wave normal and the ray vector coincide. The path of the ordinary beam is OA and the direction of the extraordinary beam is OE, which is parallel to the tangent T on the index ellipsoid at the point $x_0 z_0$. The vector $O\text{-}x_0 z_0 = n_e'$ represents the index of refraction of the wave normal of the extraordinary component. From the equation of the index ellipsoid

$$\left(\frac{x}{n_o}\right)^2 + \left(\frac{z}{n_e}\right)^2 = 1$$

and the equations of Snell's law

$$n' \sin \beta = n_o \sin \beta_o = n_e' \sin \beta_e'$$

the equations of the coordinates x_0, z_0 can be derived

$$z_o = \frac{1}{\cos \gamma} \left(n' \sin \beta - x_o \sin \gamma \right)$$

$$x_o = \frac{n_o^2 \cos \gamma}{n_o^2 \sin^2 \gamma + n_e^2 \cos^2 \gamma} \left(n' \sin \beta \operatorname{tg} \gamma \pm \frac{n_e}{n_o} \sqrt{n_o^2 \sin^2 \gamma + n_e^2 \cos^2 \gamma - n'^2 \sin^2 \beta} \right)$$

n' is the index of refraction of the adjacent medium

The direction of the tangent at this point is the derivative of the equation of the index ellipsoid

$$\tan \Phi = \frac{d_z}{d_{x(x_o, z_o)}} = -\left(\frac{n_e}{n_o}\right)^2 \frac{x_o \cos \gamma}{n' \sin \beta - x_o \sin \gamma}$$

Using Figure 2.4, the relation between the splitting angle ϵ, the angle of incidence β, and the cutting angle γ can be derived easily.

$$\epsilon = -\frac{\pi}{2} + \gamma + \beta_o + \Phi$$

$$= -\frac{\pi}{2} + \gamma + \arcsin\left(\frac{n'}{n_o} \sin \beta\right) + \arctan\left[-\left(\frac{n_e}{n_o}\right)^2 \frac{x_o \cos \gamma}{n' \sin \beta - x_o \sin \gamma}\right]$$

The equation used for the calculation of figures 2.1 - 2.4 is a special case of the last equation. There, the equation was derived for a beam of normal incidence ($\beta = 0$).

In Figure 2.5, the graphical plot of $\epsilon = f(\beta, \gamma)$ is shown for $CaCO_3$ at $\lambda = 632.8$ mμ. From this figure, it follows that an angle γ exists for which the function $\epsilon = f(\beta, \gamma)$ becomes symetric (i.e. $f(\beta) \sim f(-\beta)$ (at least for small angles of incidence β). This cutting angle γ and the corresponding splitting angle ϵ for $\beta = 0$ will be called the isotropic angles ϵ_i and γ_i. These angles can be derived from the derivative of the above equation of the splitting angle.

$$\frac{d\epsilon}{d\beta_{(\beta=0)}} = 0$$

and results in

$$\sin^2 \gamma_i = -\frac{2n_e^4 (n_o^2 + n_e^2) - n_o^4 n_e^2}{2 (n_o^2 + n_e^2) (n_o^4 - n_e^4)} \pm \sqrt{\frac{n_e^4}{n_o^4 - n_e^4} + \left(\frac{2n_e^4 (n_o^2 + n_e^2) - n_o^4 n_e^2}{2 (n_o^2 + n_e^2) (n_o^4 - n_e^4}\right)^2}$$

and

$$\epsilon_i = \arctan\left(\frac{(n_o^2 - n_e^2) \sin \gamma_i \cos \gamma_i}{n_e^2 + (n_o^2 - n_e^2) \sin^2 \gamma_i}\right)$$

Table 2.1 shows the values of ϵ_i and γ_i for $\lambda = 632.8$ mμ calculated from the equations above. The graphical plot $\epsilon = f(\beta)$ for the isotropic angle of cutting γ_i is shown in Figure 2.6 for the materials shown in Table 2.1.

Table 2.1 Isotropic splitting angle and crystal orientation of different materials.

Crystal Material	ϵ_i in degrees	γ_i in degrees
$NaNO_3$	9.17	49.34
$CaCO_3$	5.90	51.27
KH_2PO_4	1.48	53.87

The above calculations are concerned for rays with a plane of incidence coinciding with the principal plane of the crystal material. The resulting splitting angle might be called $\epsilon_{\parallel} = f(\beta)$. For light in a plane of incidence perpendicular to the principle plane, the splitting angle $\epsilon_{\perp} = f(\beta)$ is equal to $\epsilon_{\perp} = f(-\beta)$ for reasons of symmetry. However, for angles of incidence other than $\beta = 0$, $\epsilon_{\parallel}(\beta)$ is not equal to $\epsilon_{\perp}(\beta)$. This leads to a minor distortion of the shape of the spot in the output position.

3. RELATIONS BETWEEN APERTURE AND SPOT DIAMETER

3.1 CALCULATION OF THE MINIMUM APERTURE AND THE MINIMUM SPOT DIAMETER

In previous reports [1, 3], the relation between the number of positions and the aperture was calculated. This relation is recalculated for the wavelength 632.8 mμ for several numbers of stages, and several lengths of space provided for the electro optic rotators. Using the same variables, the minimum spot diameter obtainable from a light deflector with a certain aperture is recalculated also. For path length compensation, the birefringent crystal of each deflection stage is assumed to be composed of two crystals. The principle planes of these crystals are rotated 90 degrees to each other as described in the final report (3).

The minimum aperture as well as the minimum spot diameter was calculated for the maximum splitting angle and for the isotropic angle of splitting, ϵ_{max} and ϵ_i. The equations used for these calculations are the same as reported in reference (3) but are rewritten in a more general form.

a) minimum aperture

$$a = \frac{4\lambda K_1 (2^n - 1)}{K_2} \left[1 + \sqrt{1 + \frac{K_2 n_s}{4\lambda K_1^2 (2^{n/2} - 2^{-n/2})^2}} \right]$$

b) minimum spot diameter

$$\delta = \frac{n s}{\frac{a_o}{4\lambda} K_2 - 2K_1 (2^n - 1)}$$

The calculations for the minimum spot diameter δ are made assuming the aperture of the deflector a_o = 2 cm.

	ϵ_{max}	ϵ_i
$K_1 = \frac{1}{\sqrt{2} \tan \epsilon}$	$\frac{n_e n_o}{n_o^2 - n_e^2}$	$\frac{n_e^2 + (n_o^2 - n_e^2) \sin^2 \gamma_i}{\sqrt{2} (n_o^2 - n_e^2) \sin \gamma_i \cos \gamma_i}$
K_2	$n_o + \sqrt{\frac{n_o^2 + n_e^2}{2}}$	$n_o \left(1 + \frac{n_e}{\sqrt{n_e^2 + (n_o^2 - n_e^2) \sin^2 \gamma_i}} \right)$

Figure 3.1 and 3.2 show a comparison of the results of the calculations for the maximum angle of splitting ϵ_{max} and the isotropic angle of splitting ϵ_i for a 9-stage deflector whereas Figures 3.3 - 3.6 show the results for the isotropic angle of splitting ϵ_i.

3.2 MEASUREMENTS OF THE MINIMUM SPOT DIAMETER

As the equations given in Section 3.1 were derived from diffraction theory, experiments were started to check the results of these calculations. Only initial experiments can be reported as yet. The minimum spot diameter obtained from optical lenses of different focal length were measured and compared with the theoretical values.

The theoretical values were obtained from the equation of resolution:

$$\delta(f) = \frac{1.22\,\lambda\,f}{a}$$

Where $\lambda = 632.8\ m\mu$ is the wave length of the HeNe gas laser, $a = 0.4$ cm is the diameter of the laser beam , and f is the focal length of the lens being tested in these measurements.

Since this equation determines the half width of the smallest observeable point, the values obtained from the equation have to be multiplied by a factor of two in order to get the diameter of the spot as defined in the earlier report (3).

The setup used for the experiment is shown in Figure 3.7. A HeNe gas laser is used as a light source in order to obtain parallel monochrometic light ($\lambda = 632.8 m\mu$). The light beam is focussed by means of the lens and the focal point observed using a microscope with a cross hair eye piece. The diameter of the focal point is measured by using a micrometer for moving the microscope. The movement of the microscope is in a horizontal plane perpendicular to the observation direction. Figure 3.8 shows the two positions of the cross hair for measuring the diameter of the focal point. For visual observation, a high-power, neutral-density filter is used in the experiment in order to decrease the intensity of the laser beam.

The results of the measurements as well as the values obtained theoretically are shown in Table 3.2.

Table 3.2. Diameter of the focal point obtained from different lenses

Focal Length (cm)	Spot Diameters (μ)	
	Theoretical	Experimental
12.0	46.2	50
16.4	63.2	60
40.0	154.0	138

The results of the measurements are in good agreement with the theoretical values. Further experiments have to be done in order to determine the influence of the light deflector onto the diameter of the spot.

4. DETERMINATION OF THE OUTPUT POSITION

4.1 CALCULATION OF THE MINIMUM SEPARATION BETWEEN TWO ADJACENT OUTPUT POSITIONS

In order to compensate for the different optical path lengths of the ordinary and the extraordinary beams, a structure was proposed in the final report [3] in which the birefringent crystal of each stage is designed from two crystals of equal thickness. These crystals are cemented together in such a way that their principal planes make an angle of 90 degrees with respect to each other. Because of this compensation, the unit length ℓ_0 of the birefringent crystals is:

(1) For the maximum angle of splitting ϵ_{max}

$$\ell_{0\,max} = \frac{b}{\sqrt{2}\,\tan\epsilon_{max}} = \frac{\sqrt{2}\,n_e\,n_o}{n_o^2 - n_e^2}\,b$$

(2) For the isotropic splitting angle ϵ_i

$$\ell_{0i} = \frac{b}{\sqrt{2}\,\tan\epsilon_i} = \frac{n_e^2 + (n_o^2 - n_e^2)\sin^2\gamma_i}{\sqrt{2}\,(n_o^2 - n_e^2)\sin\gamma_i\cos\gamma_i}\,b$$

where b is the smallest separation or distance between two adjacent spots.

The unit lengths ℓ_{0max} and ℓ_{0i} are calculated for some values of b and different crystal materials and the results are shown in Table 4.1.

Table 4.1. Unit length of the birefringent crystals for different crystal materials and different values of minimum beam separation.

b(μ)	$NaNO_3$		$CaCO_3$		$K\,H_2PO_4$	
	ℓ_{0max} (mm)	ℓ_{0i} (mm)	ℓ_{0max} (mm)	ℓ_{0i} (mm)	ℓ_{0max} (mm)	ℓ_{0i} (mm)
10	0.042	0.044	0.065	0.068	0.260	0.275
50	0.208	0.219	0.324	0.342	1.295	1.375
100	0.417	0.438	0.649	0.685	2.595	2.750

4.2 INFLUENCE OF THE FABRICATION TOLERANCES ON THE MINIMUM SEPARATION OF TWO OUTPUT POSITIONS

The accuracy of the separation between two adjacent positions of the light deflector depends mainly on the precision of fabrication of the birefringent crystals. The influence of variation of the specifications of the KDP crystals is negligible.

From the equation:

$$b = \sqrt{2}\, \ell_o \tan \epsilon$$

the variation in b can be determined by the derivative of this equation:

$$\Delta b = \sqrt{2}\, \left[\tan \epsilon\, \Delta \ell + \ell_o (1 + \tan^2 \epsilon)\, \Delta \epsilon\right]$$

or for the relative variation.

$$\frac{\Delta b}{b} = \frac{\Delta \ell}{\ell_o} + 2\, \frac{\Delta \epsilon}{\sin 2\epsilon}$$

The variation in ϵ can be derived as a function of a change in the direction of the optic axis $\Delta \gamma$ and a change in the angle of incidence $\Delta \beta$. The latter occurs by a misalignment of the crystal surfaces relative to the incident light beam. (A variation of the parellelness of the crystal leads to a similar change in the spot position, as the misalignment of the crystal.)

For the relation:

$$\Delta \epsilon = f(\Delta \gamma, \Delta \beta)$$

the general equation of the splitting angle is used.

$$\epsilon = -\frac{\pi}{2} + \arcsin\left(\frac{n'}{n_o} \sin \beta\right) + \arctan\left[-\left(\frac{n_e}{n_o}\right)^2 \frac{x_o \cos \gamma}{n' \sin \beta - x_o \sin \gamma}\right]$$

The relation is derived by means of a Taylor series

$$\Delta \epsilon = \frac{1}{1!}\left(\frac{\partial \epsilon}{\partial \gamma} \Delta \gamma + \frac{\partial \epsilon}{\partial \beta} \Delta \beta\right) + \frac{1}{2!}\left(\frac{\partial^2 \epsilon}{\partial \gamma^2} \Delta \gamma^2 + 2\, \frac{\partial \epsilon}{\partial \gamma}\, \frac{\partial \epsilon}{\partial \beta} \Delta \gamma \Delta \beta + \frac{\partial^2 \epsilon}{\partial \beta^2} \Delta \beta^2\right) + \ldots$$

As the values of the tolerances $\Delta \gamma$ and $\Delta \beta$ are small, only the first part of the Taylor series is of practical interest. From this, it follows that

$$\Delta \epsilon_{(\beta = o)} = \frac{\partial \epsilon}{\partial \gamma_{(\beta=0)}} \Delta \gamma + \frac{\partial \epsilon}{\partial \beta_{(\beta=0)}} \Delta \beta$$

$$\Delta\epsilon_{(\beta=o)} = \left(1 - \frac{n_e^2\, n_o^2}{n_e^4 + (n_o^4 - n_e^4)\sin^2\gamma}\right)\Delta\gamma + \left(1 - \frac{n_e n_o^2 \sqrt{n_e^2 + (n_o^2 - n_e^2)\sin^2\gamma}}{n_e^4 + (n_o 4 - n_e 4)\sin^2\gamma}\right)\frac{n'}{n_o}\Delta\beta$$

For $\gamma = \gamma_m$ the derivative $\frac{\partial \epsilon}{\partial \gamma}_{(\beta=0)}$ equals zero. The same is true for $\frac{\partial \epsilon}{\partial \beta}_{(\beta=0)}$ when $\gamma = \gamma_i$

Table 4.2 shows the values of the derivatives for both cutting angles γ_m and γ_i and for different crystal materials.

Table 4.2: $\frac{\partial \epsilon}{\partial \gamma}$ and $\frac{\partial \epsilon}{\partial \beta}$ for different crystal materials.

	$NaNO_3$		$CaCO_3$		KH_2PO_4	
	γ_m	γ_i	γ_m	γ_i	γ_m	γ_i
$\frac{\partial \epsilon}{\partial \gamma}_{(\beta=0)}$	0	0,099	0	0,067	0	0,018
$\frac{\partial \epsilon}{\partial \beta}_{(\beta=0)} \frac{n_o}{n'}$	-0.08	0	-0.053	0	-0.014	0

From Table 4.2, it follows that the linear influence of the tolerances of fabrication $\Delta\gamma$ and $\Delta\beta$ is very small and may be neglected compared with the variation in length $\Delta\ell$.

Therefore the relative variation of the output position depends mainly on the accuracy of the length of the crystals.

$$\frac{\Delta b}{b} = \frac{\Delta \ell}{\ell_o}$$

5. BACKGROUND LIGHT

In addition to the primary light beam in the controlled position of the light deflector, smaller amounts of light appear in some other positions of the output surface of the deflector. In the following calculations, the background light generated in the different parts of one stage of the deflector will be called q. As explained below, the main contribution to this background light is due to the convergence of the light beam. Both crystals, the electro-optic active one as well as the birefringent crystal contribute to this background light. Some other sources of background light are the tolerances of fabrication of the crystals, the variation in amplitude of the applied voltage signal, and the bandwidth of the light to be used. As a laser is considered as a light source for the light deflector, the amount of background light from the bandwidth of the laser can be neglected.

5.1 BACKGROUND LIGHT ORIGINATING FROM THE CONVERGENCE OF THE LIGHT BEAM

5.1.1 Convergent Light In An Electro Optic Crystal

In Figure 5.1, a light beam is shown incident upon a crystal surface under an angle β. This beam normally is split into an ordinary and an extraordinary component traveling at different speeds through the crystal. Therefore, after leaving the crystal, a certain phase difference between the two components of the beam exists which leads to a change of the status of polarization. If the incident light beam is linearly polarized, after leaving the crystal, the light is elliptically polarized. The ellipticity depends on the angle of incidence and the thickness of the crystal material. Elliptically polarized light can be decomposed into two components polarized perpendicular to each other. Without any signal applied to the electro optic crystal, the component of the light which is polarized parallel to the original polarization direction is directed into the selected position. The component which is polarized perpendicular is directed into some other positions and contributes to the background light of the deflector.

From Figure 5.1, the phase difference ψ between the two components of the light beam is

$$\psi = \frac{1}{\lambda} \left(n_o d_o - n_{e'} d_{e'} + a \right)$$

where λ is the wavelength of the light, n_o and $n_{e'}$ are the ordinary and extraordinary indices of refraction, $n_o d_o$ and $n_{e'} d_{e'}$ are the corresponding optical path lengths, and "a" is the path difference occurring in the adjacent homogeneous medium. "a" can be derived from Figure 7.1 as

$$a = n' \left(d_{e'} \sin \beta_{e'} - d_o \sin \beta_o \right) \sin \beta$$

Using Snell's law of refraction

$$n' \sin \beta = n_o \sin \beta_o = n_{e'} \sin \beta_{e'}$$

and the equation of the extraordinary index of refraction for oblique incidence

$$n_{e'}^2 = n_o^2 + \left(\frac{n'}{n_e}\right)^2 (n_e^2 - n_o^2) \sin^2 \beta$$

the equation of the phase difference can be written as

$$\psi = n_o \frac{d}{\lambda} \left(\sqrt{1 - \left(\frac{n'}{n_o}\right)^2 \sin^2 \beta} - \sqrt{1 - \left(\frac{n'}{n_e}\right)^2 \sin^2 \beta} \right)$$

The amplitudes of a linear polarized convergent light beam with the plane of polarization in the y direction can be expressed as

$$x = 0$$

$$y = \sin \omega t$$

In general, for a ray of this beam incident upon the crystal at an angle β, the corresponding principal plane does not coincide with the plane of polarization of this ray. The angle between the two planes is called η. As shown in Figure 5.2, the ray is split into two components, one polarized parallel to the principal plane, the other polarized perpendicular to this plane. The two components of the ray travel through the crystal as indicated in Figure 5.1 and emerge from the crystal with a phase difference as derived above. The amplitudes of the two components after traveling through the crystal, in the x'y' coordinate system, are

$$x' = y \cos \eta = \cos \eta \sin \omega t$$

$$y' = y \sin \eta = \sin \eta \sin (\omega t + \varphi)$$

where $\varphi = 2 \pi \psi$ is the phase difference between the two components. Transformation onto the xy coordinate system leads to the following equations for the intensities of the x and y components of the light, which are the squares of the corresponding amplitudes

$$I_x = x^2 = \sin^2 2\eta \sin^2 \frac{\varphi}{2}$$

$$I_y = y^2 = 1 - \sin^2 2\eta \sin^2 \frac{\varphi}{2} = 1 - I_x$$

The total light polarized in the x and in the y direction is given by the summation over the angle η, and the angle of convergence β. The range of summation is $0 \leq \eta \leq 2\pi$ and $0 \leq \beta \leq \beta'$.

$$I_x(\beta') = \frac{1}{2\pi \beta'} \int_0^{2\pi} \int_0^{\beta'} x^2 \, d\eta \, d\beta$$

$$\frac{1}{2\beta'} \int_0^{\beta'} \sin^2 \frac{\varphi}{2} \, d\beta$$

In this calculation, the light polarized in the y direction is deflected into the selected position. The light which has its polarization direction in the x direction is the background light q (β').

q (β') is calculated by evaluating the integral by a numerical method (Simpson's rule). Figure 5.3 and 5.4 show the result of these calculations at $\lambda = 632.8$ m μ for different angles of convergence β' and varying thicknesses of the crystal.

5.1.2 Convergent Light In A Birefringent Crystal

In the birefringent crystal, a certain amount of background light is also generated when a convergent light beam is used. Figure 5.5 shows a convergent beam incident upon a birefringent crystal. The light is split into a part which travels the selected path and is polarized in the original direction and another part with a polarization direction perpendicular to the original direction. The latter part of the light is the background light.

In Figure 5.5, the surface of a crystal is shown upon which a linearly polarized convergent light beam is incident. xyz are the crystallographic axes of the crystal.

The optic axis of the crystal is identical with the z axis. x'y'z' represents the coordinate system of the crystal surface and the incident light beam. The x' axis is parallel to the x axis and the z'axis coincides with the normal N to the surface. N represents the axis of the convergent light beam as well. The angle of convergence is β', and γ is the cutting angle of the crystal.

The principal plane of a ray with the angular coordinates β, η, intersects the circular cut of the index ellipsoid of the birefringent crystal under an angle ξ relative to the x axis. This angle ξ can be determined by constructing a plane through the origin of the coordinate system in such a way that this plane is perpendicular to the incident ray. This plane is then identical with the principal plane of this ray. The equation of this plane is

$$x' \sin\beta \cos\eta + y' \sin\beta \sin\eta + z' \cos\beta = 0$$

or written in the xyz coordinate system

$$x \sin\beta \cos\eta + y (\sin\beta \sin\eta \cos\gamma + \cos\beta \sin\gamma) + z (\cos\beta \cos\gamma - \sin\beta \sin\eta \sin\gamma) = 0$$

The equation of the circular cut of the index ellipsoid of the crystal is

$$z = 0$$

These two planes intersect with each other along a line

$$z = 0$$

$$x \sin\beta \cos\eta + y (\sin\beta \sin\eta \cos\gamma + \cos\beta \sin\gamma) = 0$$

The angle between this line and the x axis, respectively x' axis is

$$\tan \xi = \frac{y}{x} = - \frac{\sin \beta \cos \eta}{\sin \beta \sin \eta \cos \gamma + \cos \beta \sin \gamma}$$

The plane of polarization of the light beam will be either in the x or in the y direction depending on whether it passes through the crystal as the ordinary or the extraordinary ray. The contrast ratio can be calculated for both cases similarly. In the case of a desired extraordinary path in the birefringent crystal, the amplitudes of the incident light beam are:

$$x = 0$$

$$y = \sin \omega t$$

Depending on the angular coordinates β and η of its rays, the light beam is decomposed into two paths x_1, and y_1, one parallel and the other perpendicular to the corresponding principal plane

$$x_1 = y \sin \xi$$

$$y_1 = y \cos \xi$$

While y_1 passes through the crystal as the extraordinary ray, x_1 passes as the ordinary ray and causes background light in an unselected position.

The intensities of the two paths of the incident light beam are the summation of the square of the amplitudes over the angles

$0 \leq \eta \leq 2\pi$ and $0 \leq \beta \leq \beta'$.

$$I_x(\beta) = \int_0^{2\pi} \int_0^{\beta'} \sin^2 \xi \, d\eta \, d\beta$$

$$I_y(\beta) = \int_0^{2\pi} \int_0^{\beta'} \cos^2 \xi \, d\eta \, d\beta = 1 - I_x(\beta)$$

Using the equation of the angle ξ derived above the background intensity can be written as

$$I_x(\beta') = q(\beta') = \frac{1}{2\pi \beta'} \int_0^{2\pi} \int_0^{\beta'} \frac{d\eta d\beta}{1 + \frac{1}{\cos^2 \eta} (\sin \eta \cos \gamma + \cot \beta \sin \gamma)^2}$$

The background light for calcite at $\lambda = 632.8$ mμ is shown in Figure 5.6.

5.2 BACKGROUND LIGHT ORIGINATING FROM THE FABRICATION TOLERANCES OF THE CRYSTALS

The amount of background light generated in the electro-optic active crystal, as well as in the birefringent one, depends on the precision of fabrication of these crystals. For the electro-optic crystal; this additional background light is a function of the deviations of at least four constants

$$q = f(\gamma, \beta, \theta_e, d)$$

and a function of the deviation of three constants for the birefringent crystal

$$q = f(\gamma, \beta, \theta_b)$$

For these functions, the constants are: γ the angle between the optic axis and the normal to the surface, β the angle of incidence, θ_e the angle between the plane of polarization of the incident light and the crystallographic x and y axes, θ_b the direction of the principle plane relative to the edges of the birefringent crystal, and d the thickness of the electro-optic crystal.

All of these constants are influenced by the precision of fabrication. An analytical determination of the contribution to the background light from these deviations will be reported in the next quarterly report. But as follows from estimates, the contributions of the tolerances of the specific values γ, β, etc. to the background light can be neglected compared to the background light generated by the convergence of the light beam. Figure 5.3, e.g. shows the influence of the variation in thickness of the electro-optic crystal. At β = 2 degrees and d = 2 mm, tha additional background light q originating from a thickness variation Δd will be $q(\Delta d) \sim 0.0002$ for $\Delta d = 0.05$ mm. The background light originating from the convergence of the light beam $q(\beta, d) \sim 0.02$ for β = 2 degrees and d = 2 mm. Therefore the influence of Δd can be neglected for small values of Δd.

5.3 BACKGROUND LIGHT ORIGINATING FROM AN AMPLITUDE DEVIATION OF THE APPLIED SIGNAL

If a signal V is applied to an electro-optic crystal properly arranged between linear polarizers, the transmitted light can be written in terms of the intensities of two components polarized perpendicular to each other

$$I_x = \sin^2 \frac{\pi}{2} \frac{V}{V_{\lambda/2}} \quad \text{and} \quad I_y = \cos^2 \frac{\pi}{2} \frac{V}{V_{\lambda/2}}$$

where $I_x + I_y = 1$ and is the intensity incident upon the electro-optic crystal, V is the amplitude of the applied signal, and $V_{\lambda/2}$ is the half wave voltage of the crystal material. For $V = V_{\lambda/2}$ the induced phase retardation in the crystal is $\lambda/2$ and the polarization direction of the incident light is rotated 90 degrees. For this case the intensities of the two components become

$$I_x = 1 \quad ; \quad I_y = 0$$

For a signal deviation of ΔV ($V = V_{\lambda/2} \perp \Delta V$) the retardation in the crystal differs from $\lambda/2$ and the light becomes elliptically polarized. The intensities of the two components change to

$$I_x = 1 - q\,(\Delta V)$$

$$I_y = q\,(\Delta V)$$

In the light deflector, only the x component of this light is deflected into the desired position whereas the y component contributes to the background light of the deflector. Written as a function of the signal deviation the y component is:

$$I_y = q\,(\Delta V) = \cos^2 \frac{\pi}{2} \left[\frac{(V_{\lambda/2} \pm \Delta V)}{V_{\lambda/2}} \right] = \sin^2 \frac{\pi}{2} \frac{\Delta V}{V_{\lambda/2}}$$

and is shown in Figure 5.7 as a function of the signal deviation.

5.4 BACKGROUND LIGHT ORIGINATING FROM THE DISPERSION OF THE HALF WAVE VOLTAGE OF THE CRYSTAL MATERIAL

The half wave voltage of the XH_2PO_4 and XD_2PO_4 crystal materials depend linearly on the wavelength of light [1]. Therefore for monochromatic light only a 90 degree rotation of plane of polarization can be achieved by applying a corresponding signal $V = V_{\lambda_o/2}$ to the crystal (λ_o is the wavelength of the monochromatic light). If the light has a half width $\Delta\lambda$, light of a wavelength λ ($\lambda - \lambda_o \div / \Delta\lambda /$) will be elliptically polarized. The intensity of this elliptically polarized light can be written as the intensities of two components.

$$I_x = \sin^2 \frac{\pi}{2} \frac{V}{V_{\lambda/2}}$$

$$I_y = \cos^2 \frac{\pi}{2} \frac{V}{V_{\lambda/2}}$$

In the light deflector, again the y component contributes to the background light of the deflector, whereas the x component is deflected into the desired position. By applying a signal $V = V_{\lambda_o/2}$ to the crystal and using the equation $V_{\lambda/2} = c\,\lambda$ as an approximation for the wavelength dependence of the half wave voltage, the intensity of the y component for a wavelength λ is

$$I_y\,(\lambda) = q\,(\lambda) = \cos^2 \frac{\pi}{2} \frac{\lambda_o}{\lambda}$$

Two different cases are considered in these calculations:

a) The light is monochromatic but differs from λ_o the wavelength which corresponds to the amplitude of the applied signal and

b) The light has a certain half width $\Delta\lambda$ centered at λ_o. The intensities are to be equal for all wavelengths in this region.

5.4.1 Monochromatic Light

For $\lambda = \lambda_o \pm \Delta\lambda$, the intensity of the y component is

$$q(\lambda_o \pm \Delta\lambda) = \cos^2 \frac{\pi}{2} \frac{\lambda o}{\lambda o \pm \Delta\lambda}$$

In Figure 5.8 the relation between the $q(\lambda_o \pm \Delta\lambda)$ and the deviation in wavelength is shown for two different wavelength λ_o

(λ_o = 546.1 mμ and λ_o = 632.8 mμ)

For small values of $\Delta\lambda$ a series expansion can be used which leads to

$$q(\lambda_o \pm \Delta\lambda) = \sin^2 \frac{\pi}{2} \frac{\Delta\lambda}{\lambda}$$

This equation is the same as the one derived in 5.3 for the voltage deviation.

5.4.2 Polychromatic Light

To determine the background light originating from polychromatic light of a half width $\Delta\lambda$, the intensity of the y component has to be integrated

$$q(\Delta\lambda) = \frac{1}{\Delta\lambda} \int_{\lambda_1}^{\lambda_2} I_y(\lambda)\, d\lambda$$

where the limits λ_1 and λ_2 are related to the half width $\Delta\lambda$ by

$$\lambda_2 - \lambda_o = \lambda_o - \lambda_1 = \Delta\lambda/2$$

Using the relation

$$q(\lambda) = \cos^2 \frac{\pi}{2} \frac{\lambda_o}{\lambda}$$

the integral can be written as

$$q(\Delta\lambda) = \frac{1}{\Delta\lambda} \int_{\lambda_1}^{\lambda_2} \cos^2 \frac{\pi}{2} \frac{\lambda_o}{\lambda}\, d\lambda$$

$$= \frac{\lambda}{2\Delta\lambda} \left[2\cos^2 \frac{x}{2} + x\left(x - \frac{x3}{3.3!} + \frac{x5}{5.5!} - \frac{x^7}{7.7!} + \dots\right) \right]_{\lambda_1}^{\lambda_2}$$

with $$x = \pi \frac{\lambda_o}{\lambda}$$

This equation will be evaluated and the results reported in the next quarterly report.

5.5 BACKGROUND LIGHT IN ONE STAGE OF THE LIGHT DETLECTOR

The background light generated in one stage of the light deflector is the algebraic sum of the different background lights described in this section. One stage of the light deflector is shown in Figure 6.1. The electro optic switch is composed of two electro-optic crystals of equal thickness in order to decrease the amplitude of the signal to be applied for 90 degree rotation of the plane polarization to half the value necessary for one crystal. This has to be considered for the determination of the influence of the thickness of the electro-optic crystals on the background light shown in Figures 5.3 and 5.4.

The total amount of background light is

$q_t = q(\beta, 2d) + q(\beta) +$	background light by the convergence of the light
$+ q(\gamma, \beta, \theta_e, d) + q(\gamma, \beta, \theta_b) +$	background light by the fabrication tolerances
$+ q(\Delta V) +$	background light by voltage deviation
$+ q(\Delta \lambda)$	background light by wavelength deviation

The values of the different terms can be obtained from the corresponding Figures 5.3, 5.4, 5.6, 5.7, and 5.8 for any desired design.

6. SPECIFICATIONS OF THE CRYSTALS FOR A 256 x 256 POSITION LIGHT DEFLECTOR

The light deflector to be built under this contract will be designed for two dimensional deflection with 256 x 256 addressable positions. This number of positions will be obtained by an 8-stage linear light deflector for the x deflection direction and another 8-stage linear light deflector for the y deflection direction arranged behind each other. Convergent light of a wavelength of $\lambda = 632.8$ m μ (the wavelength of a He Ne laser) will be used. The deflector will be compensated for the difference in optical path length between the ordinary and the extraordinary beam using the compensation method described in the final report [3]. The crystal material used for the design will be deuterated KDP (KD_2PO_4) for the electro-optic crystals and calcite ($CaCO_3$) for the birefringent crystals. As the total length of two 8-stage linear deflectors will be approximately equal to the length of a 9-stage linear deflector, the minimum aperture and the minimum spot diameter can be obtained from Figures 3.4 and 3.6 for n = 9. For a space s = 20 mm provided for the electro-optic crystals, the minimum aperture is a_i = 12 mm. The minimum aperture is derived by considering the diffraction at the entrance pupil only. Scattering from intermediate surfaces as electrodes, etc. is neglected. This scattering leads to an increase of the minimum spot diameter of the deflector. Therefore, a larger aperture of 20 x 20 mm is choosen for this design. A minimum spot diameter of $\delta_i = 10\mu$ would be the theoretical limit for an aperture of 20 x 20 mm. The light deflector will be designed for a minimum spot separation between two adjacent spots of b = 50 μ. The corresponding display area at the exit surface of the deflector will be 12.8 x 12.8 mm^2.

The angle of convergence β in the light deflector can be calculated from the total length L and the aperture a,

$$\tan \beta = \frac{a}{2L}$$

The total length L can be expressed in terms of n, s, and ℓ_o

$$L = 2[ns + (2^n - 1)\, 2\, \ell_o]$$

where n is the number of stages of the linear deflector s is the space provided for the electro-optic crystals, and ℓ_o is the unit length of the birefringent crystals. For n = 8, s = 10 mm, ℓ_o = 0.34 mm and a, = 20 x 20 mm^2 the angle of convergence will

$$\beta = 1.1 \text{ degrees}$$

The dimensions of the electro-optic crystals are shown in Figure 6.2. The electro-optic switch of each stage will be designed from two electro-optic crystals which will be arranged in series optically and electrically switched in parallel as shown in Figure 6.1. Therefore, 32 electro-optic crystals will be necessary for the 16 switches of the light deflector. The thickness of the crystal, d, is derived from Figure 5.3 for a background light of

$$q(\beta, 2d) \sim 0.01$$

Figure 6.3 shows the dimensions of the birefringent crystals. The different length ℓ_n of these crystals are calculated from the equation

$$\ell_n = 2^{n-1} \ \ell_{oi}$$

and listed in Table 6.1.

In this equation ℓ_{oi} is the unit length of calcite for a minimum separation of b = 50 μ as listed in Table 4.1. To perform the compensation of focal depths each birefringent element is composed of two crystals of equal thickness (see Figure 6.1). With the x and y deflector identical, four crystals of every length ℓ_n are needed. This makes a total of 32 crystals.

The fabrication tolerances given in Figures 6.2 and 6.3 are normal precision of optical fabrication. Only the tolerance $\Delta \ell = \pm 0.03$ mm is calculated for an accuracy in spot position of 0.1b. ($=5\mu$).

The influence of the fabrication tolerances on the background light is assumed to be negligible. Also, because the light will be a He Ne laser and therefore monochromatic, the term $(\Delta \lambda)$ in the total amount of background light in section 5.5 will be zero.

Therefore, from Figures 5.3, 5.6, and 5.7 at $\beta = 1.1$ degrees, d= 2 mm, and $\frac{\Delta V}{V} = 0.06$ the background light generated in one stage of the light deflector will be

$$q_t = 0.022$$

Table 6.1 Length of the Birefringent Crystals
(Material $CaCO_3$)

η	ℓ_n (mm)
1	0.34
2	0.69
3	1.37
4	2.74
5	5.48
6	10.98
7	21.96
8	43.92

7. ADDRESSING THE LIGHT DEFLECTOR

For many applications of the light deflector, one must know how to set the switches in order to have the light emerging from a certain position. For other applications, the inverse function if required, namely from what position does the light emerge if a certain signal is applied to the switches.

7.1 GRAPHICAL METHOD FOR OBTAINING THE RELATION BETWEEN THE OUTPUT POSITION AND THE REQUIRED SIGNAL COMBINATION

The relation between any output position and the required signal combination applied to the electro-optic switches can be obtained from the diagram shown in Figure 7.4 for an 8 x 8 position light deflector, with compensation of optical path length. This diagram is explained by means of Figures 7.1 - 7.3. In Figure 7.1, a linearly polarized light beam enters the first stage of the light deflector at "P" and is emerging from the birefringent crystal of this stage either at "0" or at "1" as shown in [3]. P-0 and P-1 are principle planes of the two parts of the crystal. The light beam emerges at "0" if no signal is applied to the electro-optic switch, or it emerges at "1" if a signal is applied and the polarization direction of the light beam is changed for 90 degrees. Therefore, symbols "1" or "0" indicate a change or no change in the status of polarization of the light beam and also indicate the status of the signal applied to the electro-optic crystal. Entering the second stage of the deflector from either one of the two positions "0" and "1" the light beam has four possible positions to leave this second stage "00", "11", "10", and "01" depending on the status of the signal applied to the second electro-optic switch. The two digits of the binary number of the position represent the status of the signal applied to the corresponding switch. The light beam is deflected along the principle planes of the crystal which are indicated by the lines 0-00, 0-10, 1-11 and 1-01. The eight positions at the exit surface are obtained by entering the last stage of the deflector at any one of the four possible positions and applying a signal "1" or "0" to the electro-optic crystal at this stage.

The convergent-beam version of the light deflector is designed for the undeflected position to be in the middle of the output surface. In this case, the controlled deflections have to be in two directions, below and above the undeflected or zero position. In order to obtain this type of deflection, the largest stage of the deflector is rotated 180 degrees relative to the deflection directions of the other stages. This design was chosen to decrease internal reflections as much as possible, since minimum internal reflection is obtained when light is normally incident on a surface.

Figure 7.2 shows a diagram of a three stage light deflector, the last stage of which is rotated 180 degrees. The diagram is derived in the same way as the one shown in Figure 7.1.

For a two-dimensional light deflector, two of these diagrams with deflections in x and y directions are superimposed as shown in Figure 7.3. Figure 7.4 shows all possible positions of an 8 x 8 position light deflector. The positions are indicated by the related x and y signal combination which must be applied to the corresponding electro-optic crystals.

This type of a diagram will be helpful in display applications of the light deflector. An example would be the determination of the signal combinations necessary for displaying any image-like information (maps, graphics, etc.) by means of the light deflector.

7.2 ANALYTICAL METHOD FOR OBTAINING THE RELATION BETWEEN THE OUTPUT POSITION AND THE REQUIRED SIGNAL COMBINATION

The graphical method for obtaining the relation between input signal and output position makes use of the actual path of the light through the deflector. Therefore, the relationship can be clearly illustrated.

For some applications of the light deflector, however, it is more useful, to have the input-output relation in an analytical form. The usefulness of this method will be shown in a later section where it is applied to the evaluation of the noise distribution of the deflector.

In the analytical method, the output position is denoted as "position address PA," and the combination of selected switches the "switch address," SA.

In the light deflector, an arbitrary electro-optic switch changes the linear polarization by rotating it 90 degrees, or by not rotating it. These are two possible states which will be called "1" and "0", respectively. The "switch address" will be written in order sequence starting with that switch which stage causes the greatest deflection. Figure 7.5 shows a 3-stage light deflector. The switches are designated S_1, S_2, and S_3; S_1 belongs to the deflection stage with the smallest deflection, S_3 belongs to the stage with the greatest deflection. The position addresses, PA, are counted binary-wise from 000 at the bottom to 111 at the top. In the adjacent column, are the switch addresses which correspond to the particular position addresses, written binary-wise in the order $S_3, S_2\ S_1$.

The task is to find the functional connection between the position address and the corresponding switch address, or the inverted connection. It is obvious from Figure 7.5 that the lowest-order bits of the two address coincide. The second-order bit of the switch address is zero if the second-order bit of the position address equals the first-order bit. The second-order bit of the switch address is 1 if the second-order bit of the position address is not the same as the first-order bit. The same is true for the third-order bit of the switch address. These features determine an exclusive "OR" function that is demonstrated in Figure 7.6 in an equivalent circuit. The functional connection between the SA's and PA's is found similarly. The circuit for this case is shown in Figure 7.7. It will be noted that in Figure 7.6 and 7.7, the first element which connects the lowest order lines of th PA with that of the SA, is shown to be a diode. However, it would be sufficient to have a straight connector.

The addressing system developed above for a one-dimensional, 3-stage deflector can be expanded in a straight forward way for a two-dimensional light deflector. All position addresses, PA now lie in one plane. We introduce x and y coordinates to distinguish the PA's which now get two binary coordinate values: PA-x and PA-y. PA-x is the horizontal coordinate and is related to SA-x, which gives horizontal deflection. PA-y and SA-y are the vertical coordinates of PA and SA, respectively. In Figure 7.8 the PA-area is shown for an 8 x 8 stage light deflector, having 256 horizontal, (x), and 256 vertical, (y), coordinate values.

The above assumed light deflector of 8 x 8 stages is under construction. In this light deflector, the eighth horizontal, and the eighth vertical deflection stage will be inverted to give downward deflection as explained in section 7.1. While deriving the circuits of Figure 7.6 and 7.7 deflection in only one direction was assumed.

However, in the equivalent circuits for this specific deflector, we put in inverters in the signal lines that correspond to the eighth deflection stages. This is shown in Figure 7.9.

A generalization of the addressing system for a n x n-stage deflector by means of the equivalent circuits is given in Figure 7.10. In the general case, the k-th stage of a deflector is inverted for downward deflection, as shown in our addressing system in the equivalent circuits of Figure 7.11.

A feature of the addressing system developed is the parity of the switching address. The parity may be defined here as "even" or "odd" referring to an even or odd number of "1's" in the SA's. The special arrangement of the deflector stages in increasing order of deflection enables us to use the parity of the SA's to classify the PA's into groups which are spatially separated. In Figure 7.5, all switch addresses with even parity occur in the lower half of the addresses and odd paritiy switch addresses occur in the upper half. In the case of a two-dimensional light deflector, there is a classification of the PA's by means of the SA-parities into four quadrants as shown in Figure 7.12. There is indicated that all position addresses PA given by PA-x and PA-y, with corresponding equal parity switch addresses (SA-x, SA-y) are placed in the same quadrant. This feature is independent on the deflection direction of one or more stages, except that the quadrants become interchanged symmetrically.

8. THE NOISE DISTRIBUTION

In Section 5, it was explained that a light beam passing through a deflector stage loses some light to the non-switched output position. This undesired light has been called background light or noise.

For a light deflector with several deflector stages in series, each stage will contribute to the total noise. This yields an attenuation of the signal intensity and an increase of background light in the output positions, or position addresses, PA. The noise problem influences such light deflector applications as display, optical printing, or as an optically access device.

The addressing system developed in Section 7.2 and the parity criteria on the switch addresses, SA, are useful tools to analyze the noise problem.

To get a convenient model for the noise analyzer, we made the assumption that each deflector stage gives an equal distribution to the total noise. This is justified by the analysis in Section 5 where the convergence of the light in the electro-optic crystals and the voltage fluctuations were found to be the main noise sources. As in Section 5, we assume unit light intensity to enter the deflector. The fraction of light of an incident ray which goes the wrong way in a deflector stage, is called q. The magnitude q is the total background light of one stage as derived in Section 5. The light that goes the right way is called p. We state that $p + q = 1$, which means that we exclude (for these considerations) light losses by absorption, reflection, and scattering.

In Figure 8.1, the noise distribution in a three-stage deflector is shown. The switch address choosen for this example is SA* — 101 what corresponds to the addressed position PA* - 011. The star on the SA and PA symbol refers to the actual switched address.

The sum of light behind each deflector stage is unity. The sums of the products of p and q behind each stage come out to be the terms of the binomial expansion $(p + q)^n$. That gives for the output of the third stage $(p + q)^3$. As indicated in Figure 8.1, we will call

$p^3 = I_o$ relative intensity in the addressed position PA*

$p^2q = I_1$ first order noise

$pq^2 = I_2$ second order noise

$q^3 = I_3$ third order noise

In the other rows of the Figure 8.1 the PA's and SA's and the parity of the SA's are listed. It is obvious that the PA's with first order noise, I_1, and third order noise, I_3, have odd parity in their SA's and I_o and I_2 have even parity. By taking a PA* with odd SA* parity, one finds that the second order noise, I_2, also occurs in PA's with odd SA-parity. Furthermore one sees that the SA's of those PA's in which first order noise, I_1, occurs differ in one digit from SA*. The SA's of the PA's with second order noise, I_2, differ in two digits from the addressed switch

address SA*. The analog is true for the third order noise I_3. The multitude of each noise level I_m is given by the number of combinations of the n bits in the SA*, inverted m at a time that is $\binom{n}{m} = \frac{n!}{(n-m)!\,m!}$.

For our example we have n = 3 and we find for

m	I_m	multitude
0	I_o	1
1	I_1	3
2	I_2	3
3	I_3	1

The numbers of multitude $\binom{n}{m}$ simply are the binomial coefficients of the expansion given above. The sum of these binomial numbers equals 2^n which is the total number of position addresses achieved by an n-stage digital light deflector.

In the case of a two dimensional light deflector having n x-deflection stages and also n y-deflection stages there are 2n different noise levels. The noise is distributed upon the four parity quadrants of Figure 7.12. If a position address PA* is chosen with a switch address SA* -x of odd parity, and SA*-y of even parity, we can state the following facts. The PA* lies in the quadrant "odd-even" of Figure 7.12. Even indexed noise levels such as I_2; I_4; etc. occur only in this quadrant and in the diagonal quadrant. The odd indexed noise levels as I_1; I_3; I_5; etc. occur only in the off-diagonal quadrants "even-even" and "odd-odd". For reason of symmetry in the latter case there is a half-to-half distribution. This does not hold for the address quadrant and its diagonal quadrant. The distribution can be calculated by combinatoric means with the requirement that the parity does not change. These calculations have been made for the addressed quadrant for two dimensional deflectors of 10; 12; 14; 16; 18; 20 stages. The results are coefficients C_{2k} which give the multitude of the even indexed noise levels in the address quadrant; these coefficients are listed in Table 8.1. The sum of all the noise in the address quadrant and the relative intensity I_o in the PA* is plotted in Figure 8.2 as a function of the noise q in each deflector stage. The parameter of the curves is the total number of deflector stages 2n. These curves determine the sum of the relative intensity of the noise in the address quadrant and the relative intensity in the addressed PA*, that is the relative signal intensity.

The macroscopic noise distribution shows that there is no first order noise in the quadrant in which the signal occurs. Second order noise will be the brightest background noise. If we assume an 8 x 8 stage light deflector and a noise of q = 0.1 in each deflector stage, we find the relative signal intensity $I_o = 0.185$, and the noise intensities $I_1 = 0.021$ and $I_2 = 0.002$. That means the brightest noise spots in the addressed quadrant have only about one hundredth of the signal intensity. If we allow a 20 per cent noise contribution in each deflection stage, that is q = 0.2, we find $I_o = 0.028$, $I_1 = 0.007$, $I_2 = 0.0018$, with a ratio $I_o / I_2 \sim 15$. In this case, the signal

TABLE 8.1

C_{2K}	10 Stages	12 Stages	14 Stages	16 Stages	18 Stages	20 Stages
C_2	$2\binom{5}{2}$	$2\binom{6}{2}$	$2\binom{7}{2}$	$2\binom{8}{2}$	$2\binom{9}{2}$	$2\binom{10}{2}$
C_4	$2\binom{5}{4}+\binom{5}{2}^2$	$2\binom{6}{4}+\binom{6}{2}^2$	$2\binom{7}{4}+\binom{7}{2}^2$	$2\binom{8}{4}+\binom{8}{2}^2$	$2\binom{9}{4}+\binom{9}{2}^2$	$2\binom{10}{4}+\binom{10}{2}^2$
C_6	$2\binom{5}{4}\binom{5}{2}$	$2+2\binom{6}{4}\binom{6}{2}$	$2\binom{7}{6}+2\binom{7}{4}\binom{7}{2}$	$2\binom{8}{6}+2\binom{8}{4}\binom{8}{2}$	$2\binom{9}{6}+2\binom{9}{4}\binom{9}{2}$	$2\binom{10}{6}+2\binom{10}{4}\binom{10}{2}$
C_8	$\binom{5}{4}^2$	$2\binom{6}{2}+\binom{6}{4}^2$	$2\binom{7}{6}\binom{7}{2}+\binom{7}{4}^2$	$2+2\binom{8}{6}\binom{8}{2}+\binom{8}{4}^2$	$2\binom{9}{8}+\binom{9}{6}\binom{9}{2}+\binom{9}{4}^2$	$2\binom{10}{8}+2\binom{10}{6}\binom{10}{2}+\binom{10}{4}^2$
C_{10}	0	$2\binom{6}{2}$	$2\binom{7}{6}\binom{7}{4}$	$2\binom{8}{2}+2\binom{8}{6}\binom{8}{4}$	$2\binom{9}{8}\binom{9}{2}+2\binom{9}{6}\binom{9}{4}$	$2+2\binom{10}{8}\binom{10}{2}+2\binom{10}{6}\binom{10}{4}$
C_{12}		1	$\binom{7}{6}^2$	$2\binom{8}{4}+\binom{8}{6}^2$	$2\binom{9}{8}\binom{9}{4}+\binom{9}{6}^2$	$2\binom{10}{2}+2\binom{10}{8}\binom{10}{4}+\binom{10}{6}^2$
C_{14}			0	$2\binom{8}{6}$	$2\binom{9}{8}\binom{9}{6}$	$2\binom{10}{4}+2\binom{10}{8}\binom{10}{6}$
C_{16}				1	$\binom{9}{8}^2$	$2\binom{10}{6}+\binom{10}{8}^2$
C_{18}					0	$2\binom{10}{8}$
C_{20}						1

$\binom{N}{M}$ are the binominal numbers. It is defined: $\binom{N}{M}=\frac{N\,(N-1)(N-2)\ldots(N-M+2)(N-M+1)}{M!}$

has 15 times the intensity of the brightest noise spot in the addressed quadrant. These are very favorable conditions for display application of the light deflector. Optical printing applications are also favored by this noise distribution. However, if a single integrating light detector is used for signal detection, the noise sums as given Figure 8.2 would distort the desired signal, and more sophisticated detection circuitry must be devised.

9. CRYSTAL RESONANCES

The electro-optic effect is closely related to the piezoelectric effect. Therefore, applying a voltage to the crystal in general will cause a piezoelectric deformation. The crystal will have resonance frequencies according to its elastic properties, its shape, and its size.

In the deflector, $KD_2 PO_4$ crystal plates are employed which are 45° z cuts, as shown in Figure 6.2. The response of such a crystal in an electric field in z direction will be a deformation along the crystal's edges.

If this crystal becomes excited by a a-c voltage that matches its resonant frequency, the crystal will oscillate with a high amplitude even at a low driving voltage. As the piezoelectric deformation is connected with a piezo-optic effect, an undesired resonant excitation of the electro-optic crystals to piezoelectric oscillations would bring the deflector out of control. To avoid that, the resonance frequencies have to be known. Depending on the crystal mounting, there will be a damping of the piezoelectric oscillations. Maximum damping is highly desired.

Experiments were started to measure the resonance frequency and the damping influence for three kinds of mounting as shown in Figure 9.1.

a) Free crystal attached to the electrodes with a silicone oil film to fill the air gap.

b) Crystal attached to the electrodes immersed in silicone oil.

c) Crystal cemented to the electrodes with EPON812 +DTA*, cured at 65°C for 10 hours.

The setup for the measurements is shown in Figure 9.2. The light source is a Philips 8V, 50-watt projection bulb, the light filter a 10 $m\mu$ bandwidth interference filter with the center frequency at 543 $m\mu$. The polarizer and analyzer were polaroid foils. The quarterwave plate also was a dichroic foil and was set to introduce a 90° phase shift to the light incident on it. Thus the combination of the electro-optic crystal and the quarterwave plate operated at the quarterwave point in the sine square transmission curve to give maximum response. The photomultiplier tube is a DuMont model 6467. The sine-wave generator is a Hewlett Packard model 650 A. The amplifier is a Krohn-Hite DC A - 10 (R) model The current probe is a 456 A - Hewlett Packard model. The oscilloscope is a 555 type Tektronix scope.

The results of the measurements are listed in Table 9.1. The results show that the damping of the cemented crystal is the highest compared to the other kinds of mounting.

The resonance experiments will be continued with high voltages applied as well as with square voltage pulses to look for the resonance excitement by Fourier components of the square pulses.

* see Section 10

TABLE 9.1

Resonant frequencies of KD_2PO_4 crystal (2 x 2 x 0.1 cm^3) in various mountings.

Type of Mounting	Resonant Frequency Kc/s	Amplitude Ratio	
a	10	0.54	
	43	0.54	amplitude detected
	50	1	amplitude detected
	56	0.36	amplitude detected
	62	0.45	
	123		phase detected
	195		phase detected
b	60	1	amplitude detected
	72	0.1	amplitude detected
	170		phase detected
c	51	1	amplitude detected
	104		phase detected

The amplitude ratios are normalized signal amplitudes I/I max.

10. ELECTRODE CEMENTING

The switching of the electro-optic crystal requires transparent electrodes on both surfaces of the crystal. The light deflector uses many electro-optic crystals in series. This requires very high transparency electrodes. Besides that, the electrodes must be good conductors to provide high-speed switching up to the megacycle range. There are no electrodes available with transmissivities higher than 90 percent which can be deposited onto the crystal and which have reasonable electric properties. Therefore, electrodes which are melted upon a glass or quartz substrate are attached to the crystal. Neither the crystal surface nor the electrode surface are so flat they will fit together without a tiny gap. An air-gap will cause an electrical breakdown that will eventually destroy the crystal. The electrode must be cemented to the crystal with a conductive cement to prevent electrical breakdown.

The cementing of the electrodes will make up a sandwich as shown in Figure 10.1. First, lets discuss the electrical properties of that electrode-crystal sandwich.

The crystal has a dielectric constant of $\epsilon_c = 50$ and its specific resistance is about $2 \times 10^{+10}$ ohm centimeters. The dielectric constant of the cement is about $\epsilon_L = 2.5$ and its specific resistance somewhere between 10^{+6} and 10^{+15} ohm centimeter.

The analog circuit for the electrode-crystal sandwich is shown in Figure 10.2. The crystal capacitance C_C is in series with the cement capacitance C_L. The respective resistors R_C and R_L, due to the material conductivities, are in parallel to the capacitances. The charging and discharging process of the capacitors depends on the time constants $\tau_c = \epsilon_o \epsilon_c \rho_c = R_C C_C$ of the crystal, and $\tau_L = \epsilon_o \epsilon_L \rho_L = R_L C_L$ for the cement. With the values above we have $\tau_C = 100$ msec. If we assume $\tau_L = \tau_C$, we have the case that at all times the ratio of the voltages V_c/V_L is constant and is only dependent upon the ratio of the respective capacitances:

$$\frac{V_c}{V_L} = \frac{C_L}{C_C}$$

V_C is the voltage on the crystal, and V_L the voltage on the cement layer.

For $\tau_L \ll \tau_C$, the voltage on C_L will drop to zero very fast causing all voltage to lie on the crystal. This case is highly desirable for very low frequency switching as well as for high-speed switching.

For $\tau_L \gg \tau_C$, the voltage across C_L will grow to about the supply voltage within the time τ_C, leaving the crystal uncharged. That happens if the switching cycle time is greater than τ_C. Therefore, this case is not applicable for very-low-speed switching. The maximum switching cycle time should be smaller than 1 percent of τ_C which is about one millisecond.

Since the light deflector under construction is to be operable at very low switching speeds as well as at high switching speeds, τ_L must be less than τ_C, that is τ_L must be as small as possible.

The second electrical feature to consider is the actual voltage on C_L:

$$V_L = \frac{C_C}{C_L} \quad V_C$$

To switch the crystals economically $V_C/V_L = 100$ is a reasonable figure. We assume $\tau_C = \tau_L = 10^{-1}$ seconds, for the worst allowable case. The capacitance C_C of KD*P crystals of 0.2 cm thickness and 4 cm^2 cross section is 100 $\mu\mu$f. From the voltage ratio $V_C/V_L = 100$ we get the capacitance of the cement layer as $C_L = 10^4$ $\mu\mu$f.

The breakdown voltage of the cement should be large enough to stand the applied voltage $V_L = V_C/100$.

The dielectric constant of most transparent cements is in the range of $\epsilon_L \sim 2$ to 10. The time constant $\tau_L = \epsilon_o \epsilon_L \rho_L$ gives for the highest value of the dielectric constant of $\epsilon_L = 10$, the specific resistance to $\rho_L = 10^{11}$ ohm centimeters.

The required capacitance $C_L = 10^4$ $\mu\mu$f gives us for a minimum dielectric constant of $\epsilon_L = 2$ a thickness d of the cement layer of d = 0.72 micron. The switching voltage V_C for the deflector will be about 2000 volts. Due to $V_C/V_L = 100$, we get $V_L = 20$ volts. For a cement layer thickness of 0.72 microns, this gives a field strength of 28×10^4 V/cm which is 700 volts per mill (VPM). That is about double the value of the breakdown voltage one can find for most cements. The parameters for the cement selection, therefore, are:

a. high dielectric constant to get a high C_L

b. low resistivity, $\rho_L < 10^{11}$ ohm centimeters

c. dielectric strength as high as possible at least 300 VPM.

d. chemically neutral

c. not water dissolved or hygroscopic

d. lowest light absorption for laser-light frequencies

e. no shrinking of the cement, to avoid stress of the crystal

f. cementing below 150 centigrade (300° F)

The last five points lead to polymers and it turned out that epoxy resins seemed to be the most promising cements if used in special formulation. The dielectric constant for epoxy resins is between $\epsilon_L = 2.5$ to 3.5, the dielectric strength for recommended formulations is between 250 and 450 VPM and the resistivity for normal formulations is greater than 10^{11} ohm centimeter. However, ρ_L is very sensible to the formulation of the compounds and the curing procedure.

The following epoxy resins have been investigated with respect to their resistivity. Various formulations of the resin components for different curing procedures have been investigated. Most of the cements were two-component epoxies.

It is well known that the insulating property of a cured polymer is better than that of the components. Unbalancing of the formulation, therefore, will give different dielectric properties.

From literature tables, the most promising epoxy resins were chosen as:

	Supplier
ECCOGEL 1265	Emerson-Cuming, Inc.
STYCAST 1264	Emerson-Cuming, Inc.
ECCOBOND 45	Emerson-Cuming, Inc.
EPON 812 + DIETHELENETRIAMINE (DTA)	Miller Stephenson Chemical Co.
HE - 79	Eastman Kodak Co.
HE-F-4	Eastman Kodak Co.

which have the following property

	Resistivity in ohm centimeter	Dielectric Constant ϵ	Dielectric Strength in volts per mil
ECCOGEL 1265	10^{12}	3	
STYCAST 1264	10^{14}	3.5	
ECCOBOND 45	3.10^{13}	3.2 - 2.9	410

EPON 812+DIETHELELETRIAMINE was chosen because of its high content of hydrochlorine that could possibly give low resistivities in unbalanced formulations.

HE-79 and HE-F-4 were taken into consideration because it is used for electrode cementing by electro-optic crystal vendors.

The procedure for making samples was simply to cut square samples off the cured formulation. The square samples were electroded with silver paint. The resistance was measured by a high-voltage ohm meter.

Only formulations that become rigid, semi-regid, or flexible after curing have been used for measurements. Sticky or syrupy cement is not considered useful for electrode cementing.

Table 10. 1 shows the results on the test of the previously listed epoxy resins for various formulations and curing procedures. With respect to the resistivity, EPON 812 + DIETHYLENETRIAMINE (DTA) in the formulation 12. 5:1 by volume, cured at room temperature ofr 3 days and heated to 65° C for !0 hours, showed the best results. Therefore, this material has been chosen for more specific tests on the resistivity and on the dielectric strength.

The measurements were done on cement layers from 10 to 100 micron thickness. The mounting for the samples is shown in Figure 10.3 The cement layer is in between 2 gold plated glass substrates. The gap width is provided by an intervening layer of mylar foil. Various curing procedures were followed. The voltage was applied in small steps up to the breakdown at some samples. Only d-c voltage has been applied. The results are listed in Table 10.2.

EPON 812 + DTA in the formulation 12:1 by volume cured for 3 days at room temperature and after that heated for 10 hours at 65° C, gave the most promising result with respect to the resistivity and the dielectric strength.

These results will hold for d-c voltage and very low switching speeds. However, they have to be confirmed for high speed switching. Work is going on to find out the cement's properties in the high-frequency range.

TABLE 10. 1

Sample No.	Material	Formulation	Curing Process	Status	Resistivity ohm. cm	Remarks regarding Color
1		1:0.6	A + C	e		
2		1:0.8	A + C	c	$>10^{12}$	
3	ECCOGEL	1:1	A + C	b	$>10^{12}$	light yellow to colorless
4	1265 A + B	1:1.2	A + C	c	$>10^{12}$	
5		1:1.5	A + C	d		
6		1:0.2	C	b	8×10^{11}	
7		1:0.4	C	a	$>10^{12}$	greenish to colorless
8	STYCAST	1:0.6	C	b	$>10^{12}$	
9	A + B	1:0.8	C	d		
10		1:1	C	d		
11		1:0.25	A	e		
12		1:0.5	A	a	$>10^{12}$	
13	ECCOBOND 45	1:0.75	A	a	$>10^{12}$	yellow to orange
14	A + B	1:1	A	b	$>10^{12}$	
15		1:1.5	A	c	$>10^{12}$	
16		1:2	A	d		
17	EPON 812	6:1	A + D	a	6×10^{11}	Orange
18	+ DIETHELENE-	8:1	A + D	a	1×10^{10}	Orange
19	TRIAMINE (DTA)	10:1	A + C	a	2.2×10^{9}	Yellow to orange
20		12.5:1	A + C	b	2.4×10^{8}	light yellow
21		15:1	A + C	c	7×10^{7}	yellow-greenish
22		20:1	A + C	d		
23		12.5:1	A + D	b	5×10^{6}	yellow, curing at
24		12.5:1	A + C + D	b	2×10^{7}	higher temperature darkness
25		12.5:1	A + C + D	b	4×10^{9}	color.
26	HE-79 A + B	100:2	A + D	a	4×10^{11}	
27			A + C + D	a	7×10^{11}	colorless
28	HE-F-4,		A	d		
29	one component		A + C	b	$>10^{12}$	

TABLE 10. 1 (continued)

curing process:	A:	3 days room temperature
	B:	5 hours at 65°C
	C:	10 hours at 65°C
	D:	evacueted before curing
status:	a:	rigid
	b:	semi regid
	c:	flexible
	d:	sticky (viscous)
	e:	not homogeneous

TABLE 10.2

Electrical properties of EPON 812 + DTA in formulation 12:1 by weight. All samples are cured for 3 days at room temperature followed by 10 hours at 65° C. The breakdown voltage was applied only for 2 seconds.

Sample No	Curing Proc.	Thickness μ	Resistivity (low voltage) ohm . cm	Resistivity at 100 volts ohm. cm	Resistivity at 200 volts ohm. cm	Breakdown Voltage Volts	Dielectric Strength VPM
1		80	2.5×10^9	9×10^9	10×10^9	>500	
2		46	3.2×10^9	1.7×10^9	2×10^9	550	270
3		23	6.5×10^8	7.6×10^9	10.5×10^9	450	490
4		56	3.7×10^8	1.7×10^9	2.4×10^9	> 600	
5		25	6.3×10^8	4.8×10^9	6.9×10^9	450	450
6		38	2.6×10^8	1.1×10^9	3×10^9	500	330
7		34	2.2×10^8	1×10^9	1.7×10^9	400	290
8		40	3.2×10^8	2.7×10^9	2.7×10^9	500	310
9		11	1.1×10^9	4.7×10^9	9×10^9	300	680

11. HIGH SPEED ELECTRONIC SWITCHES

In order to switch the light beam from one output position of the light deflector to another, the polarization direction of the beam has to be changed for 90^{o} in at least one of the electro-optic switches. This change is accomplished by applying (or removing) the half-wave-length voltage $V_{\lambda/2}$ to (or from) at least one of the electro-optic crystals. As pointed out in reference 2, the energy F to be stored or to be removed from one electro-optic switch for these operations is

$$F = \frac{1}{2} \epsilon \epsilon_o \frac{a^2}{t} V^2_{\lambda/2}$$

where:

ϵ_o	absolute dielectric constant of vacuum
ϵ	relative dielectric constant of crystal material
t	thickness of the crystal
$V_{\lambda/2}$	half-wavelength voltage of the crystal material
a	aperture of the deflector

Using the most recent data of Sliker and Burlage,[5] for deuterated KD*P material, $\epsilon = 50$, $V_{\lambda/2} = 3.5$ kv at $\lambda = 632.8$ mμ, in a crystal of a = 2 cm aperture and t = 0.2 cm thickness . This energy amounts to

$$F = 0.55 \text{ m joules}$$

In a typcial way of operation, at ν deflections per second, each KD*P crystal will be charged in the average $\nu/2$ times per second. At the same rate, $\nu/2$, the energy F has to be removed. If F is removed by dissipation, then the power consumption W of each electro-optic switch at different deflection rates amounts to:

ν in defl/sec	W in watts
10^2	27.5×10^{-3}
10^3	0.275
10^4	2.75
10^5	27.5
10^6	275

At 4×10^4 defl/sec W exceeds 10 watts, and at some limit this method of operation becomes uneconomical.

It was pointed out in reference 2, that the economical range can be extended to much higher deflection rates by using special circuitry in which removal of the

switching voltage is accomplished by restoring the electric energy rather than by dissipating it. In this case, in the KD*P crystals only a small fraction of the energy is dissipated, and this is related to the loss tangent of the material. At ν deflections per second, corresponding to a sinusoidal operation at the frequency $\nu/2$, the power W_{sin} dissipated in each KD*P crystal is

$$W_{sin} = 2\pi \frac{\nu}{2} \epsilon \epsilon_0 \frac{a^2}{t} V^2 \lambda/2 \tan \delta$$

The tan δ of deuterated KD*P was not yet reported in the literature. It is expected to be similar to that of normal KDP. According to V. Hippel [6] the latter is tan $\delta \leq 5 \times 10^{-4}$ for frequencies between 10^4 and 10^7 cps. Sterzer et. al. [7] reports tan $\delta = 7.5 \times 10^{-3}$ at X band frequencies. Assuming tan $\delta = 10^{-3}$, the power dissipated at ν

ν in cps	W_{sin} in watts
10^2	0.34×10^{-3}
10^3	3.4×10^{-3}
10^4	34×10^{-3}
10^5	0.34
10^6	3.4
10^7	34

It is the subject of this section to describe circuits with restoring capability.

11.1 HIGH VOLTAGE TRANSIENT TYPE SWITCH

The basic principle of the high-voltage, transient-type switch (HVTTS) is shown in Figure 11.1. A tank capacitor C_T and the crystal capacitor C_C are connected through inductance L. These components constitute an oscillation circuit. Two high-voltage diodes D_1 and D_2 are provided at the ends of the inductance. They are inserted in a polarity so as to stop the backflow of charge from the capacitors when these are charged to the maximum voltage. Electronic switches S_1 and S_2 bridge the blocking diodes for switching and unswitching the crystal C_C. These switches can be laid out for unidirectional current flow, because in the opposite direction the current flows through diodes D_1 and D_2. Diode D_3 connects a supply voltage V_s to the circuit, which compensates for losses of the stored energy.

In order to describe the functioning of the HVTTS, we assume $C_T = C_C$ and that losses will occur only in resistance R_C inside the crystal. We further assume a random switching operation of the crystal with the restriction, that switching is initiated at periodic clock times.

Figure 11.2 shows the time chart of the circuit during one switching operation. The first line shows the voltage V_T at the tank capacitor C_T, the second line shows the voltage VC at the crystal, the third and fourth line the status of switches S_1 and S_2 respectively. The fifth line shows the time dependence of the sinusoidal supply voltage. At time t_o capacitor C_T is charged to a positive voltage $V_T(t_o)$, the crystal is uncharged, switches S_1 and S_2 are not conductive. This status is consistent, as diodes D_1 and D_3 do not allow discharge of C_T. At time t_1 switch S_1 is made conductive with the effect that C_T discharges through S_1, L, and D_2. The differential equation of this process is

$$-L \frac{di}{dt} = \left(\frac{1}{C_T}\right)\left(\int i\,dt\right) + \left(\frac{1}{C_C} \int i\,dt\right)$$

With the boundary conditions i = 0 and $V_T = V_T(t_o)$ at $t = t_o$ the integral of that equation becomes

$$V_C(t) = V_T(t_o) \frac{C_T}{C_T + C_C} \left[1 - \cos \sqrt{\frac{C_T + C_C}{L_C + C_C}} (t - t_1)\right]$$

At the time $t_2 = t_1 + \pi \sqrt{L \frac{C_T C_C}{C_T + C_C}}$, the voltage

across C_C arrives at $V_C(t_2) = V_T(t_o)$, and C_T is totally discharged. There the oscillation is stopped as S_2 is nonconductive and C_C cannot discharge through D_2. Thus, Switch S_1 can be made nonconductive at a time t_3 after t_2. Due to the finite loss resistance R_C, C_C discharges slightly to $V_C(t_4)$. The corresponding voltage drop is exaggerated in Figure 11.2.

The pulse is ended at time t_4, when switch S_2 is made conductive. Then the electric charges flow back to the tank C_T in a corresponding process. At time t_5, crystal C_C is discharged to $V_C(t_5) = 0$, tank capacitor C_T is charged to $V_C(t_5) = V_C(t_4) < V_T(t_o)$, a voltage slightly smaller than the original value $V_T(t_o)$. This deviation is compensated by the power supply. Diode D_3 becomes conductive only if the supply voltage V_S exceeds V_T. This happens at time t_6. Between t_6 and t_7, the tank condensor C_T is recharged to the peak value of the supply voltage which is equal to the rated value $V_T(t_o)$. Thus the cycle is completed.

From the described process, we learned:

1) The width of the pulses can be arbitrarily adjusted. If the supply voltage is pulse shaped rather than sinusoidal, the pulse width may be up to 3/4 of the cycle time.

2) The amplitude of the pulses at the crystal depends on the voltage $V_T(t_o)$ across the tank capacitor and on the ratio $\frac{C_T}{C_T + C_C}$ of tank and crystal

capacities. If $C_T = C_C$, the amplitude of the pulse at the crystal is equal to $V_T(t_o)$. If $C_T >> C_C$, the amplitude of the pulse at the crystal approaches twice the tank voltage $V_T(t_o)$.

3) At $C_T = C_C$, both switches S_1 and S_2 and all diodes have to stand the full voltage necessary for switching the electro-optic crystal. At $C_T >> C_C$, both switches, and diode D_1 have to stand only half that voltage.

4) The rise and decay times of the pulses are $t_2 - t_1 = t_5 - t_4 = \pi\sqrt{L\,\frac{C_T C_C}{C_T + C_C}}$. For obtaining a rise time of 1 μ sec at $C_C \approx 500$ $\mu\mu$f and $C_T >> C_C$, the inductance assumes a reasonable value of 200 μh.

5) As stated before the switches S_1 and S_2 may be unipolar. However, they must withstand a voltage as large as the switching voltage of the crystal.

In order to study the basic principle and main problems of the HVTTS, we built a very-low-speed model suited for hand operation. Switches S_1 and S_2 were push-button switches, the inductance L = 4.8 h with a serial resistance R_L = 150 ohms, D_1 and D_2 were type 1N645 diodes. Diode D_3 was replaced by a switch by which capacitor C_T could be connected to a d-c voltage for charging. The crystal was simulated by an ordinary capacitor large enough to yield a sufficient time constant when probed by an electronic voltmeter of 2×10^8 to ohms input impedance. Figures 11.3 to 11.5 show the experimental results for different values of C_T and C_C. In these figures, the ideal course of voltage V_C at the crystal for sequential operations is plotted as dotted line; the experimentally obtained voltage as a broken line. The rise and decay times are omitted in the figures. The quantity $Q = \frac{1}{R_S}\sqrt{L\,\frac{C_T + C_C}{C_T C_C}}$ is the calculated Q value of a resonant circuit under the assumption that the resistive losses of the inductance and the diodes (in forward direction) are comprised in a serial resistor R_s.

Figure 11.3 shows the experimental results for

$C_T = C_C = 30$ μf, L = 4.8 h, $R_s = 1.4 \times 10^3$ ohms

Leading and trailing edges $\pi\sqrt{L\,\frac{C_T C_C}{C_T + C_C}} = 3 \times 10^{-2}$ sec

Q value $= \frac{1}{R_s}\sqrt{L\,\frac{C_T + C_C}{C_T C_C}} = 0.4$

Result: C_C is charged to only $V_C = 0.55\ V_S$ rather than to the ideal value value $V_c = V_s$. Oscillation of the electric charge from C_T to C_C is too much damped in R_s. For better operation, Q has to be increased.

Figure 11.4 shows the experimental results for

$C_T = C_C = 0.1$ μf, L = 4.8 h, $R_s = 1.4 \times 10^3$ ohms

Leading and trailing edges $\pi\sqrt{L\,\frac{C_T C_C}{C_T + C_C}} = 1.5 \times 10^{-3}$ sec

$$\text{Q value} = \frac{1}{R_s}\sqrt{L\,\frac{C_T + C_C}{C_T\,C_C}} = 7$$

Results: At this Q value, C_C is charged to $V_C = 0.9\ V_S$, only 10 percent less than the ideal value.

After unswitching, the crystal remains partly charged to $V_C = 0.15\ V_S$ during period II. In subsequent unswitched positions (IV, VI, ...) V_C increases more and more. This disturbing effect is caused by the foltage drop at resistance R_S during the unswitching operations. For elimination means have to be provided to discharge the crystal during pulse pauses.

Figure 11.5 shows the experimental results for

$C_T = 30\ \mu f >> C_C = 0.1\ \mu f$, $L = 4.8$ h, $R_s = 1.4 \times 10^3$ ohms

Leading and trailing edges $\pi\sqrt{L\,\frac{C_T\,C_C}{C_T + C_C}} = 2 \times 10^{-3}$ sec

$$\text{Q value} = \frac{1}{R_s}\sqrt{L\,\frac{C_T + C_C}{C_T\,C_C}} = 5$$

Result: Making $C_T >> C_C$, indeed yields voltage doubling at the crystal.

The results of the experiments indicate the feasibility of the HVTTS. However, they also indicate the importance of a large Q value of the circuit, i.e. low loss resistances of the actual components.

To take into account these loss resistances, we derived the transient function of a circuit as shown in Figure 11.6. During the process of switching the crystal C_C current flows through the components which are drawn in solid lines. Those drawn in broken lines get into action during the unswitching process. However, as the components used for unswitching are equal to those used for switching, the equation to be derived for switching will be valid for unswitching too.

In Figure 11.6 is

R_{SW} the serial resistance of switch S_1 (resp. S_2) in the conductive condition.

R_L the serial resistance of the inductance L

R_D the forward resistance of Diode D_2 (resp. D_1)

R_T the parallel loss resistance of the tank capacitor C_T

R_C the parallel loss resistance of the crystal C_C.

$C_C R_C$ and $C_T R_T$ are the time constants for self discharging of the crystal and the tank capacitors, respectively. As pointed out in the final report [3] (in connection with the electrode problem), the time constant $R_C C_C$ of KD*P is in the order of

2×10^{-2} sec, that of a good capacitor $R_T C_T$ is much higher. This means that for times much shorter than the respective time constants, C_C and C_T do not discharge through their parallel resistances, and for switching rates larger than 1,000 operations/sec these resistances can be neglected. The differential equation of the transient function then is:

$$-L \frac{di}{dt} = (R_{SW} + R_L + R_D)\, i + \left(\frac{1}{C_T} + \frac{1}{C_C}\right) \int i\, dt$$

With the abbreviations:

$$R_{SW} + R_L + R_D = R_S \qquad \frac{C_T C_C}{C_T + C_C} = C_E$$

$$\frac{1}{R_S} \sqrt{\frac{L}{C_E}} = Q \qquad \omega_o^2 = \frac{1}{L C_E}$$

and the boundary conditions

$$i = o \quad \text{and} \quad \frac{di}{dt} = \frac{V_T(o)}{L} \quad \text{at} \quad t = o$$

one finally obtains

$$V_C(t) = V_T(o) \frac{C_T}{C_T + C_C} \left[1 - e^{-(R_s/2L)t} \left(\sqrt{\frac{1}{\frac{4L}{C_E R_S^2} - 1}} \sin \sqrt{\frac{1}{LC_E} - \frac{1}{4} \frac{R_S^2}{L^2}}\, t + \cos \sqrt{\frac{1}{LC_E} - \frac{1}{4} \frac{R_S^2}{L^2}}\, t \right) \right]$$

$$V_T(o) \frac{C_T}{C_T + C_C} \left[1 - e^{-(\omega_o/2Q)t} \frac{2Q}{\sqrt{4Q^2 - 1}} \cos \left(\omega_o \sqrt{1 - \frac{1}{4Q^2}}\, t - \arctan \frac{1}{\sqrt{4Q^2 - 1}} \right) \right]$$

The transient function is a damped cosine function, the frequency ω of which is slightly changed compared to the frequency ω_o of the undamped function with $Q = \infty$. If we neglect the change of frequency $\left(\frac{\omega_o - \omega}{\omega_o} < 1\% \text{ for } Q > 3.5 \right)$, then the rise

time τ_R of a switching pulse is the time in which the value of the cosine goes from +1 to -1, or the half of its period $T_o/2$:

$$\tau_R = \frac{T_o}{2} = \frac{\pi}{\omega_o}$$

The pulse amplitude, approached at $t = \tau_R$, can be approximated as

$$\frac{V_C(\tau_R)}{V_T(o)} \approx \frac{C_T}{C_T + C_C} \left(1 + e^{-(\pi/2Q)}\right)$$

Figure 11.7 shows the pulse amplitudes in dependence on the Q value for $C_T = C_C$ and for $C_T >> C_C$. The figure shows that $Q \geq 5$ will be sufficient for reasonable operation of the HVTTS.

11.2 SECOND HARMONIC PHASE MODULATION SWITCH

Another approach of a high-speed switch for the electro-optic crystals is the Second Harmonic Phase Modulation Switch (SHPMS). Its basic diagram is shown in Figure 11.8. In this switch, the switching energy oscillates continuously back and forth between the crystal C and the firmly coupled coils L_1 and L_2 at a rate of twice the deflection rate. However, depending on the sequence in which switches S_1 and S_2 are operated, the crystal is charged first to a positive and then to a negative voltage or vice versa. The light source must be strobed at appropriate clock intervals, when the crystal is charged to the first maximum value of the voltage, which is either

$$V_C = +\frac{1}{2} V_{\lambda/2} \text{ or } V_C = -\frac{1}{2} V_{\lambda/2}$$

The operation of the SHPMS can best be described by using its time chart, Figure 11.9. There the first line shows the voltage V_C at the crystal for a switching sequence "1" - "1"-"0". The clock periods are marked by fat vertical lines and the arrows indicate the strobing times. The second and the third lines show the conditions of the switches S_1 and S_2, respectively. "0" means "nonconductive", "1" means "conductive". Times during which the switch can be either "0" or "1" are drawn in two dotted lines.

It is assumed that at $t < t_o$ all switches are nonconductive, the crystal C is discharged ($V_C = 0$) and no current flows through the inductances L_1 and L_2. At $t = t_o$, switch S_1 is made conductive. A current starts flowing through S_1 and L_1 which charges the crystal to $V_C(t_1) = +2V_1 = +1/2\ V_{\lambda/2}$.

As the current flows back from the crystal through diode D_1, switch S_1 can be switched to "0" somewhere between time t_1 and t_2.

Inductances L_1 and L_2 are firmly coupled. As indicated in Figure 11.8 by the dots, they are coupled in opposite polarity. Therefore, at t_2, when the crystal is

just discharged and the energy of the oscillator is located in the inductances, the left side of L_1 is at the potential + $1/4\ V_{\lambda/2}$. This means that the left side of L_2 must be at the potential - $1/4\ V_{\lambda/2}$. Therefore, there is no voltage drop across the switches S_1 and S_2 between the inductances L_1 and L_2 and the dc voltages V_1 and V_2.

At this time, t_2, switch S_2 is made conductive. The current through D_1 changes to the path through S_2 and the crystal starts oscillating around the d-c voltage $V_2 = -1/4\ V_{\lambda/2}$. At $t = t_3$, the crystal assumes the negative peak voltage $V_C(t_3) = -2\ V_2 = -1/2\ V\lambda/2$. At this time, switch S_2 can be switched to "0" as the current now reverses and flows back through D_2. At time t_4, the crystal had once oscillated around the d-c level $V_1 = +1/4\ V_{\lambda/2}$ and once around $V_2 = -1/4\ V_{\lambda/2}$. One clock cycle is finished. At the time of the strobing pulse, it was charged to $+1/2\ V_{\lambda/2}$, this representing the "1" condition.

During the second clock cycle, the crystal shall again be switched to the "1" condition. Therefore at $t = t_4 = t'_o$ the crystal again is switched first by S_1 through L_1 to V_1 and in the second step at $t = t'_2$ through L_2 to V_2. It oscillates during the first half of this clock cycle again around the d-c voltage $V_1 = +\frac{1}{4} V_{\lambda/2}$ and during the second half around $V_2 = -\frac{1}{4} V_{\lambda/2}$.

During the third clock cycle, a "0" signal shall be applied to the crystal. In this case, the crystal is first switched to the negative and then to the positive loop. Therefore, switch S_2 is switched to "1" (or kept in "1" condition) at time $t = t''_0 = t'_4$. It is switched to "0" somewhere between t''_1 and t''_2. By switching S_1 to "1" at time t''_2, the crystal oscillates in the positive loop. The light is strobed at time t''_1, at which the crystal is charged to $V_C = -1/2\ V_{\lambda/2}$.

The following properties of the SHPMS differ mainly from those of the HVTTS.
Advantageous properties:

The switches S are operated only at times where the voltage across them as well as the current through them are zero.

During each clock period the crystal is charged half time positively and half time negatively. As the mean charge of the crystal stays zero, the principle of the SHPMS allows voltage transformation. In that case low voltage components could be used for switching.

Disadvantageous properties:

The sinusoidal shape of the signal requires strobing of the deflected light beam.

The "1" signal is a voltage of amplitude $+\frac{1}{2} V_{\lambda/2}$ rather than $+V_{\lambda/2}$, the "0" signal - $1/2\ V\lambda/2$ rather than 0. This requires an additional constant bias of the birefringence of the electro-optic crystals, such as a quarter-wave plate combined with each KD*P crystal.

The frequency of the applied signal is twice the frequency of the maximum deflection rate, or four times the average signal rate of the HVTTS.

We plan to devote further work to both of these approaches for high-speed electronic switching of the digital light deflector.

CONCLUSIONS

The purpose of the work done under this contract is to develop digital light deflectors, particularly to design a model with 256 x 256 output positions and to investigate electronic circuits for high-speed crystal switching.

For this purpose, general calculations of the optical and electro-optical properties of light deflectors have been performed. These calculations show that sodium nitrate may be advantageously used in the deflector because of its optical properties. Since this material can be grown artificially, we recommend that production of optical quality sodium nitrate be encouraged and fostered to ensure adequate sources of supply.

The calculations also yield the specifications of the electro-optic and birefringent crystals for a 256 x 256 positions deflector. Because sodium nitrate crystals are not yet readily available, the model will be built with calcite crystals. These and the electro-optic KD*P crystals will be ordered according to the evaluated specifications.

Further investigations were concerned with the problem of addressing the deflector output. Graphical and analytical approaches relating the output position to the input signal are reported.

Consideration of light exiting from unswitched positions yields an important result about the distribution of background light (noise) over the output screen. No noise of first order intensity is found in that quadrant of the screen from which the controlled beam exits. The different levels of noise have a special distribution over the quadrants of the output screen. This can be used to improve the signal to noise ratio in many applications.

Methods of mounting the electro-optic crystals can be determined by measurements of the frequency response. Different optical cements were investigated for attaching the semitransparent electrodes to the electro-optic crystals. These investigations will be continued.

Two circuits for high-speed electronic switching of electro-optic crystals are discussed. Their properties will be further investigated, to determine which is better suited for application to the deflector.

REFERENCES

1. W. Kulcke, H. Fleisher, "Use of Optical Masers in Displays and Printers", Quarterly Progress Report No. 1, 7 January through 6 April 1963 IBM Poughkeepsie, New York

2. W. Kulcke, H. Fleisher, "Use of Optical Masers in Displays and Printers", Quarterly Progress Report No. 2, 7 April 1963 through 6 July 1963 IBM Poughkeepsie, New York

3. W. Kulcke, H. Fleisher, "Use of Optical Masers in Displays and Printers", Final Report, 7 July 1963 through 6 October 1963 IBM Poughkeepsie, New York

4. H. Fleisher, K. Kosanke, "Use of Optical Masers in Displays and Printers", Supplement to Final Report 7 October through 31 December 1963 IBM Poughkeepsie, New York

5. T. R. Sliker, S. R. Burlage, Journal Applied Physics 34, 1837, 1963

6. A. R. v. Hippel, Dielectric Materials and Applications, Technical Press of MIT and John Wiley and Sons, Inc. 1954 p. 301

7. F. Sterzer, D. Blattner, S. Miniter, Journal Optical Society of America 54, 62, 1964

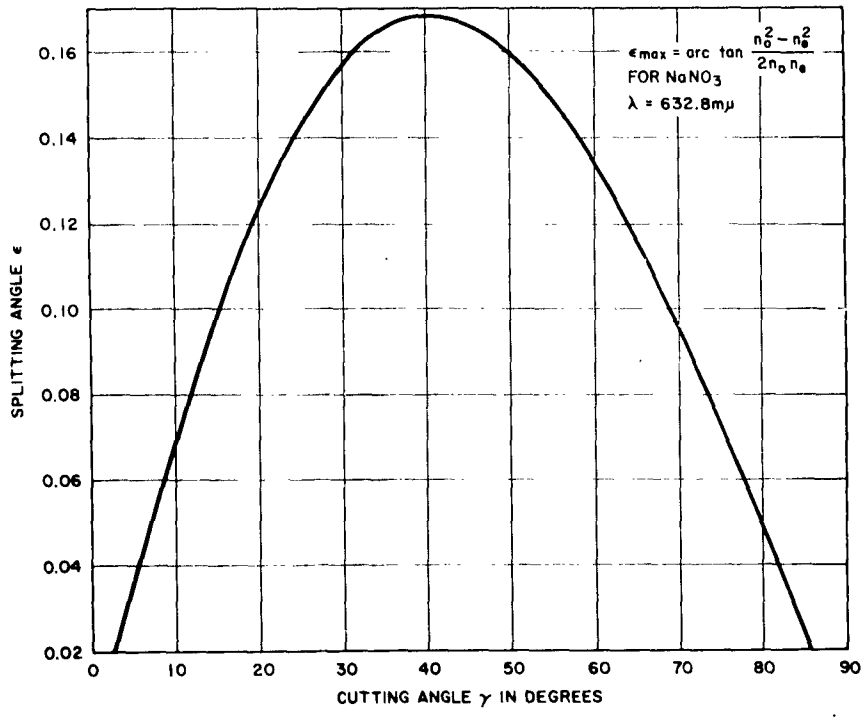

Figure 2.1. Orientation of birefringent crystals for maximum angle of splitting of ordinary and extraordinary rays.

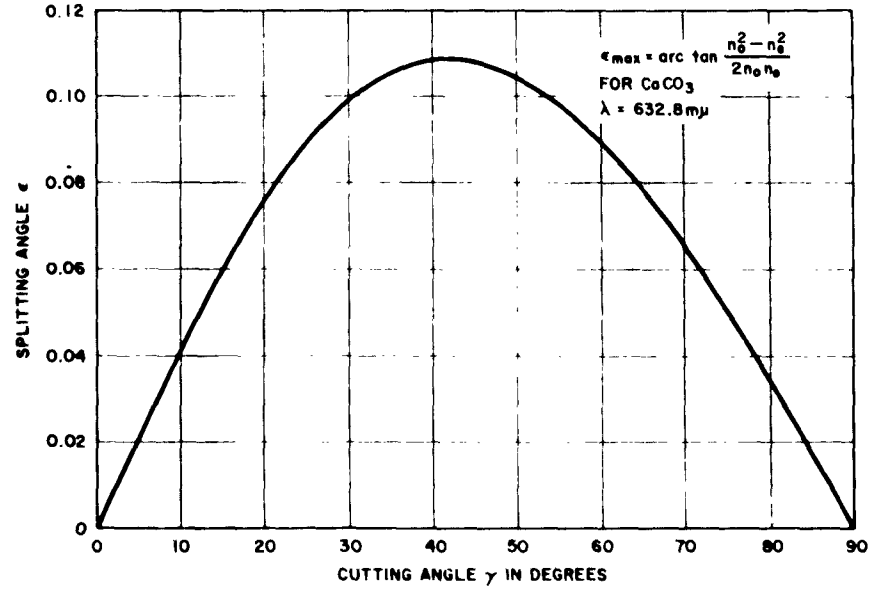

Figure 2.2. Orientation of birefringent crystals for maximum angle of splitting of ordinary and extraordinary rays.

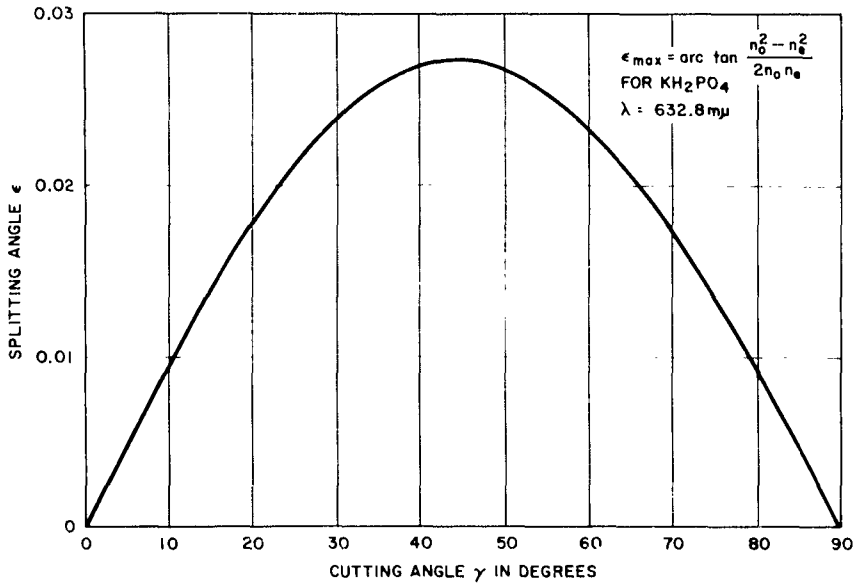

Figure 2.3. Orientation of birefringent crystals for maximum angle of splitting of ordinary and extraordinary rays.

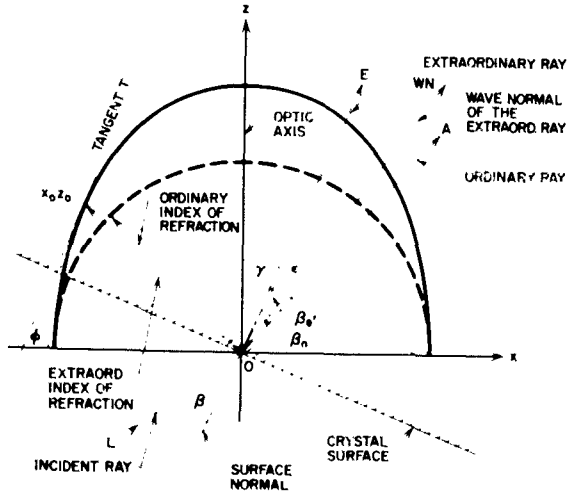

Figure 2.4. Angle of indicence between ordinary and extraordinary ray for oblique incidence and arbitrary cutting angle.

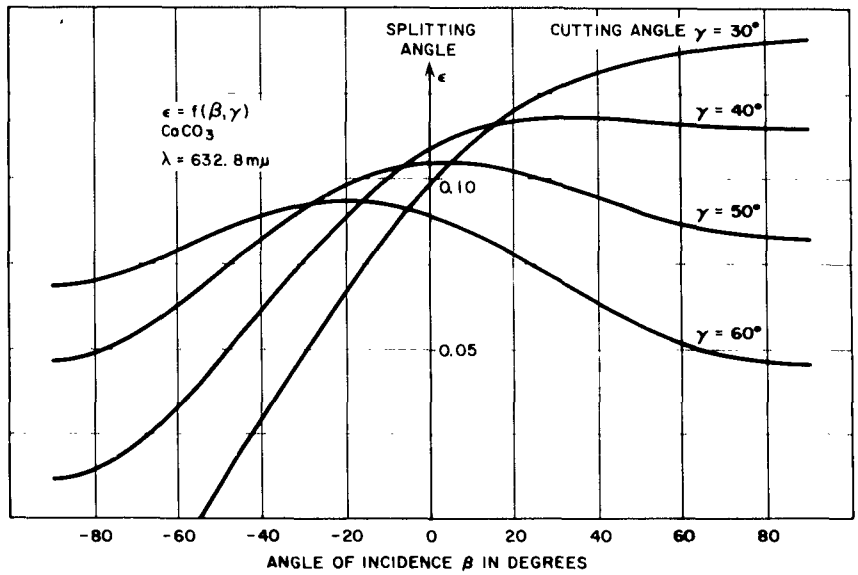

Figure 2.5. Dependence of splitting angle of calcite on orientation and angle of incidence.

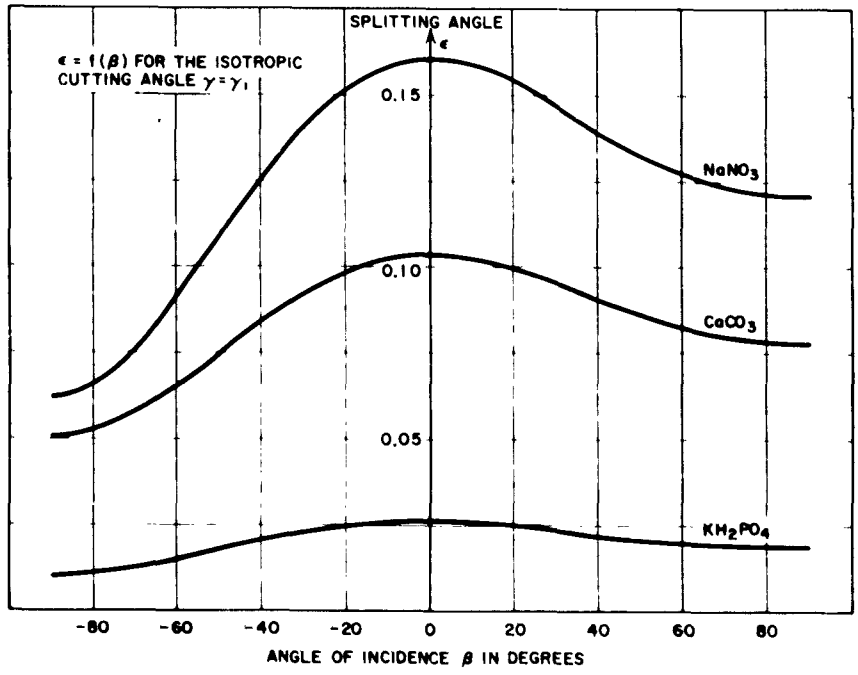

Figure 2.6. Orientation of birefringent crystals for isotropic angle of splitting.

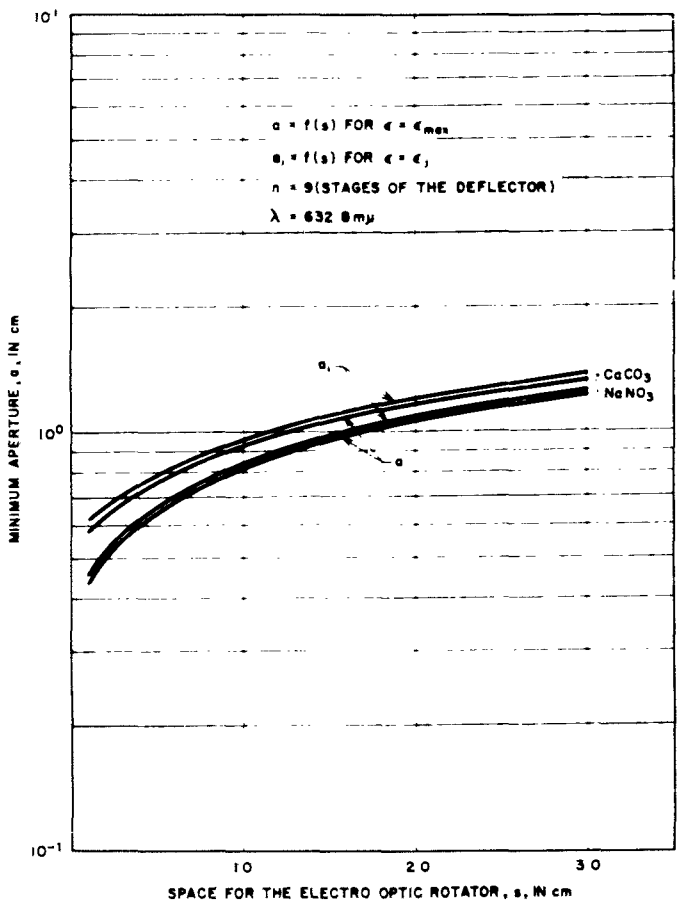

Figure 3 1. The minimum aperture for a nine-stage light deflector oriented either for the maximum splitting angle or for the isotropic one.

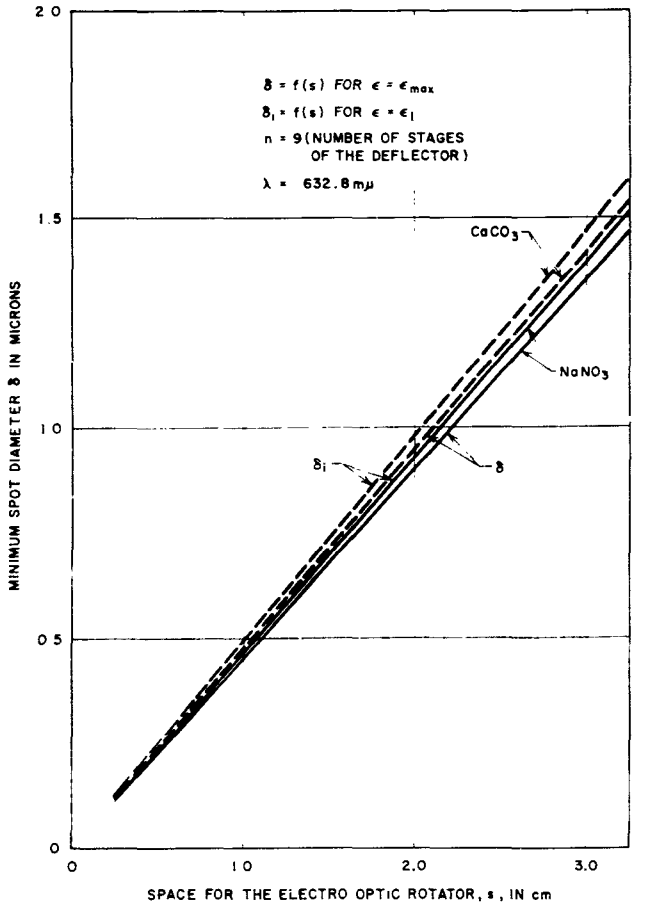

Figure 3.2. The minimum spot diameter for a nine-stage light deflector oriented either for the maximum splitting angle or for the isotropic one.

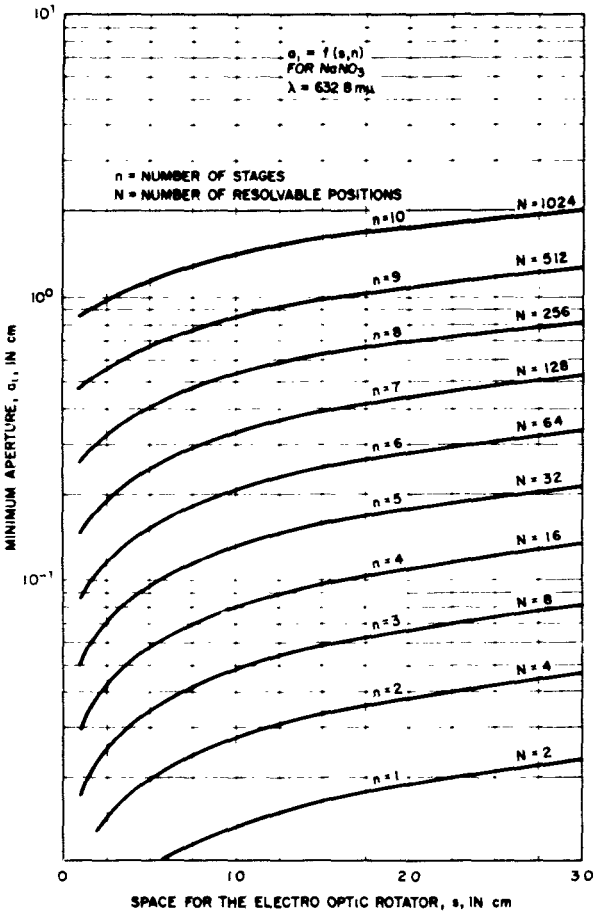

Figure 3.3 Minimum aperture of the convergent beam light deflector for N resolvable spots calculated for the isotropic angle of splitting.

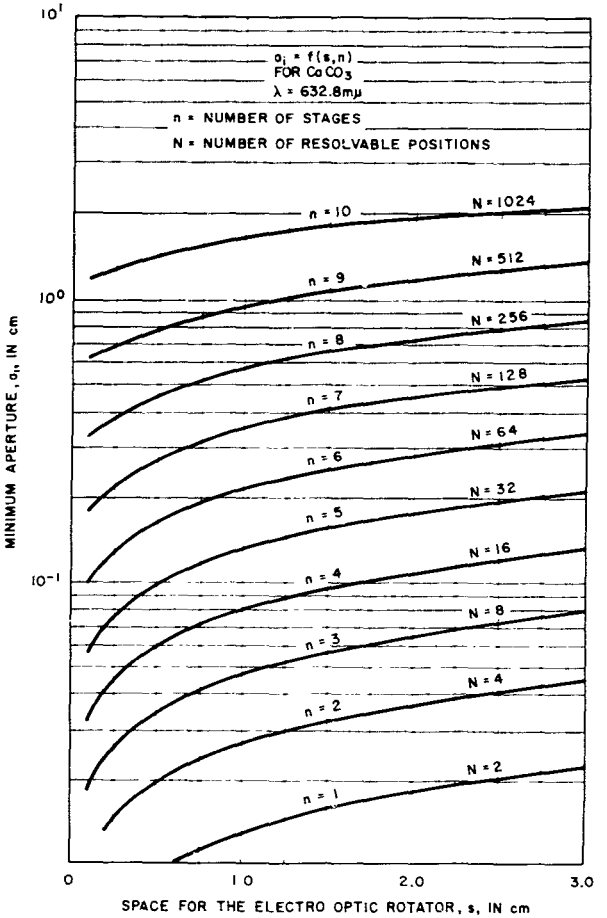

Figure 3.4. Minimum aperture for the convergent beam light deflector for N resolvable spots calculated for the isotropic angle of splitting.

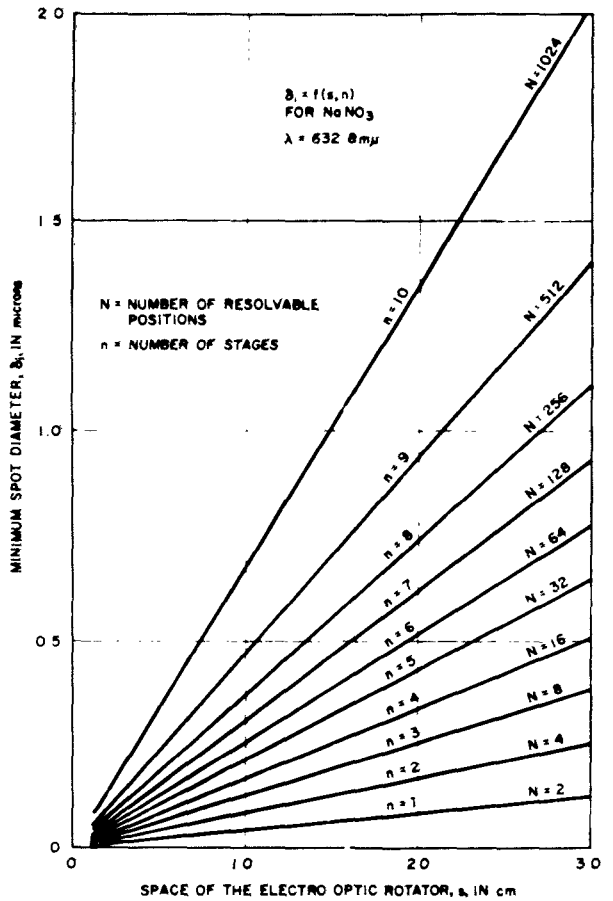

Figure 3.5. Minimum spot size of a convergent beam light deflector for N resolvable spots for the isotropic angle of splitting.

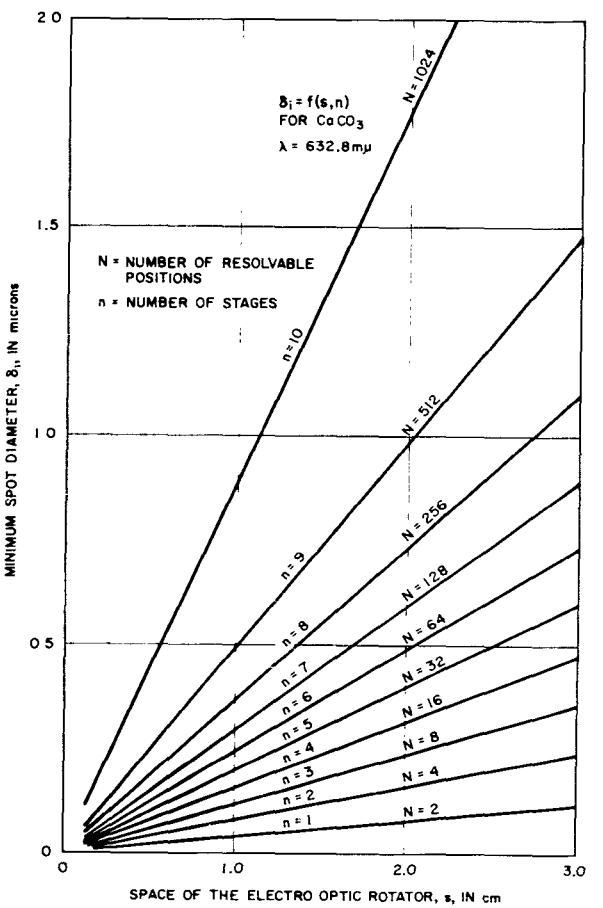

Figure 3.6. Minimum spot size of a convergent beam light deflector for N resolvable spots for the isotropic angle of splitting.

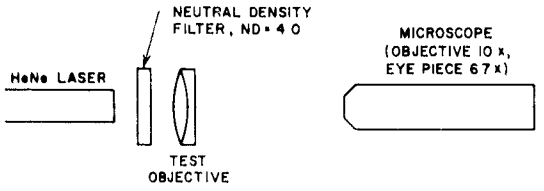

Figure 3.7. Experimental setup for diffraction measurements.

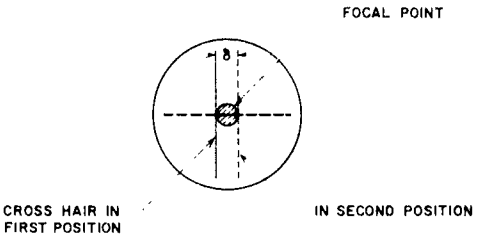

Figure 3.8. Measurement of the spot diameter. (Viewed into the microscope.)

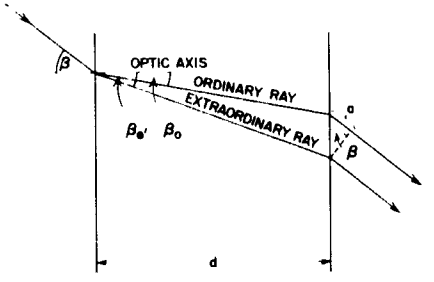

Figure 5.1. Phase relation between the ordinary and extraordinary ray in an electro-optic crystal.

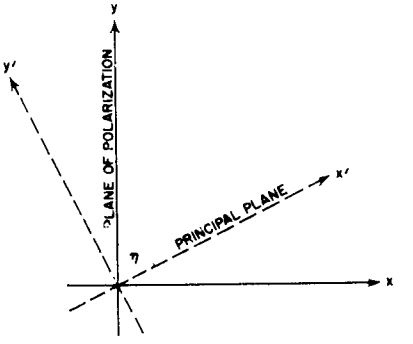

Figure 5.2. Ordinary and extraordinary components of a linearly polarized light beam obliquely incident upon an electro-optic crystal.

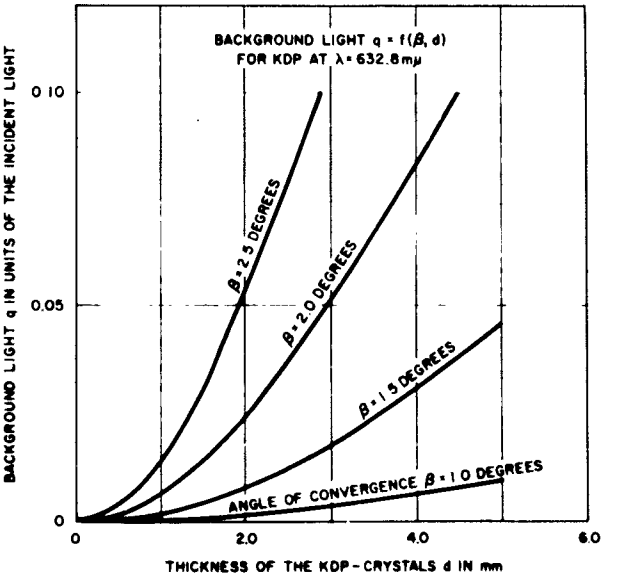

Figure 5.3. Background light of a convergent beam in KDP.

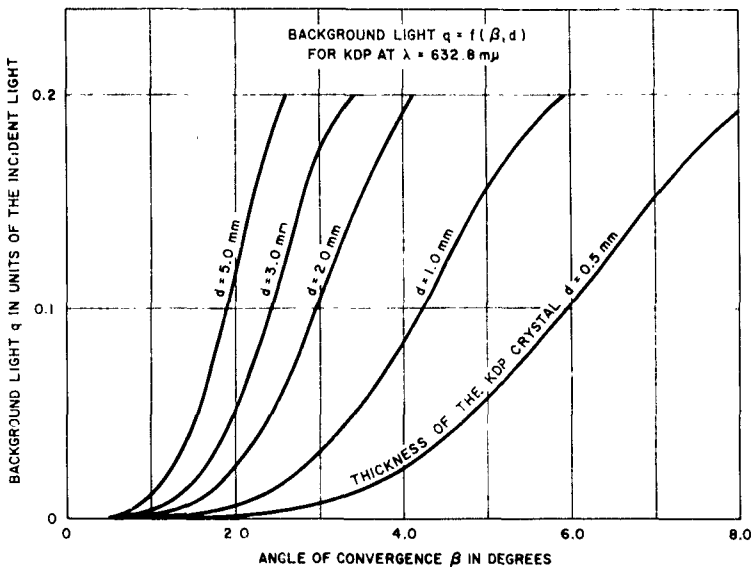

Figure 5.4. Background light of a convergent beam in KDP.

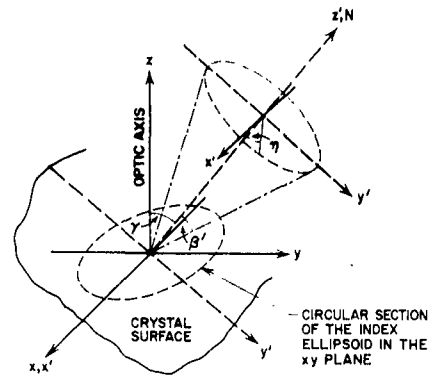

Figure 5.5. Principle plane in a birefringent crystal for oblique incidence.

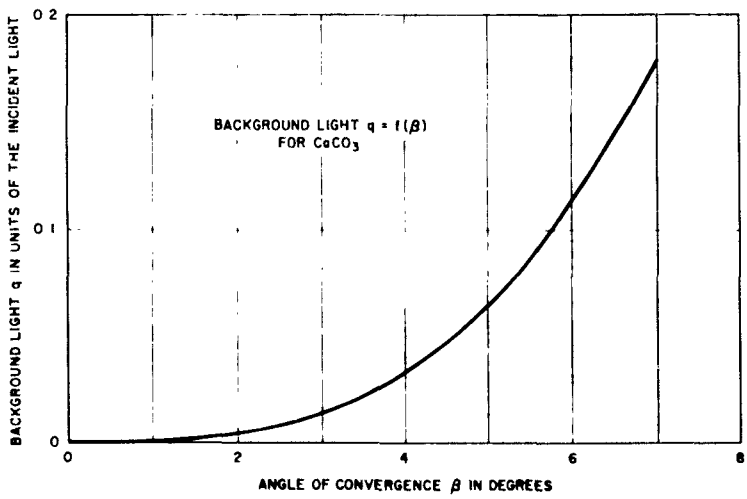

Figure 5.6. Background light of a convergent beam in calcite.

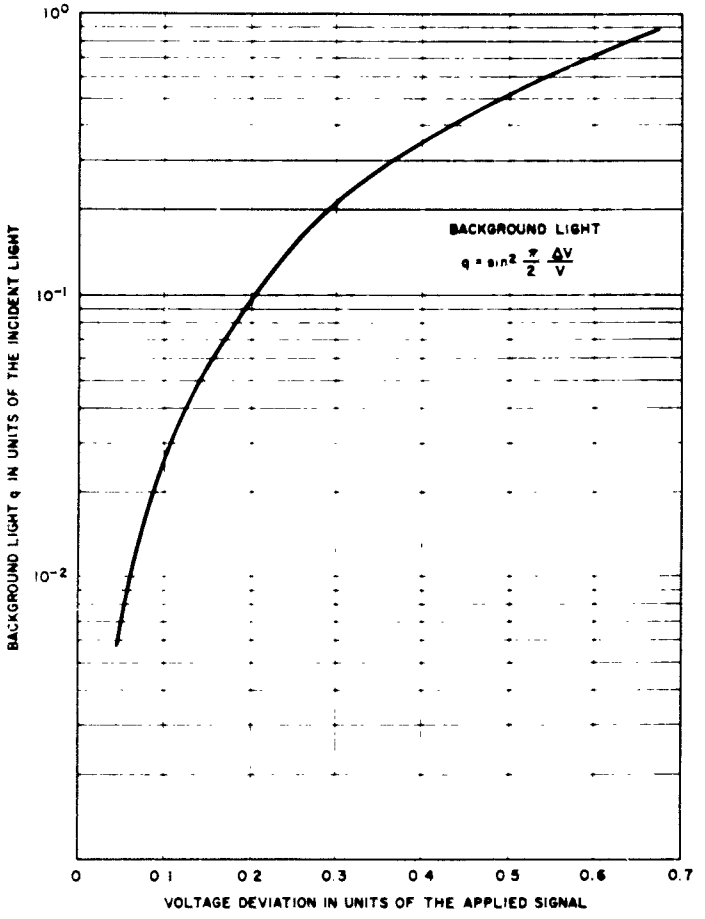

Figure 5.7. Influence of the deviation in switching voltage on the background light.

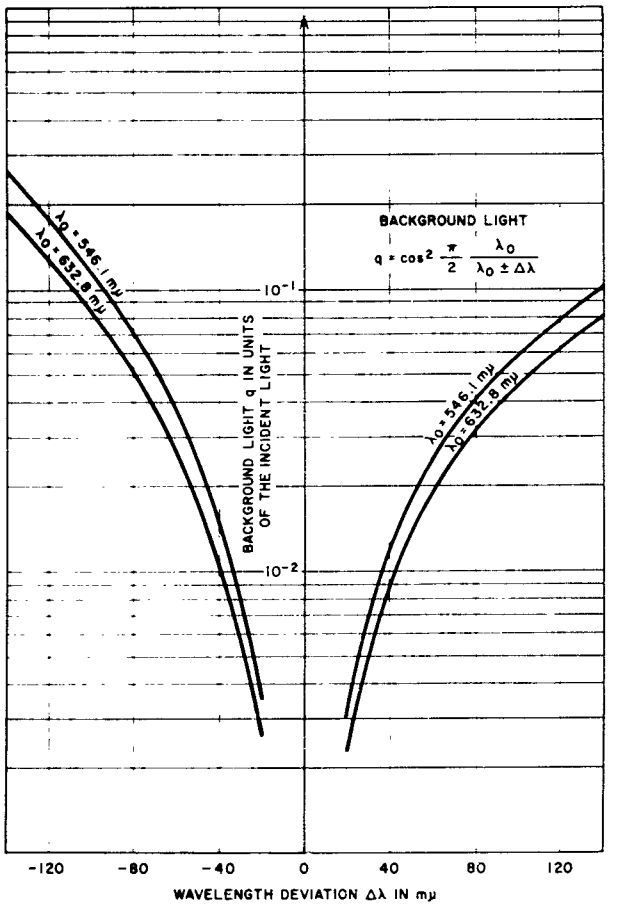

Figure 5.8. Background light of a light beam with a definite bandwidth.

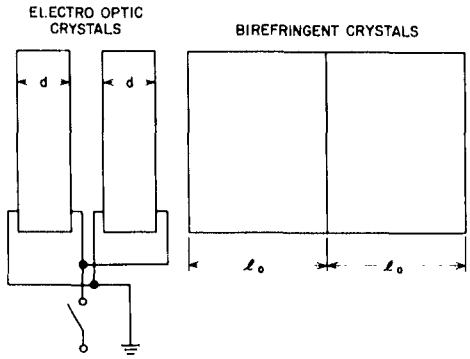

Figure 6.1. One stage of the light deflector.

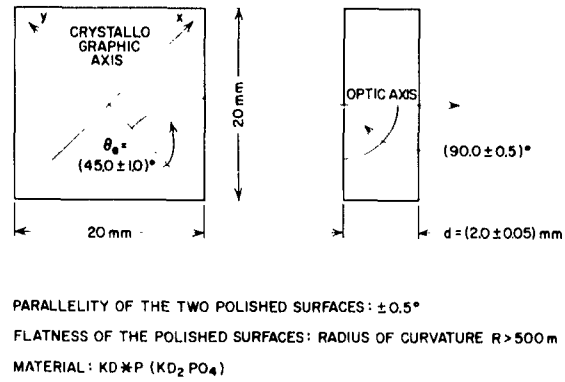

Figure 6.2. Dimensions of the electro-optic crystal.

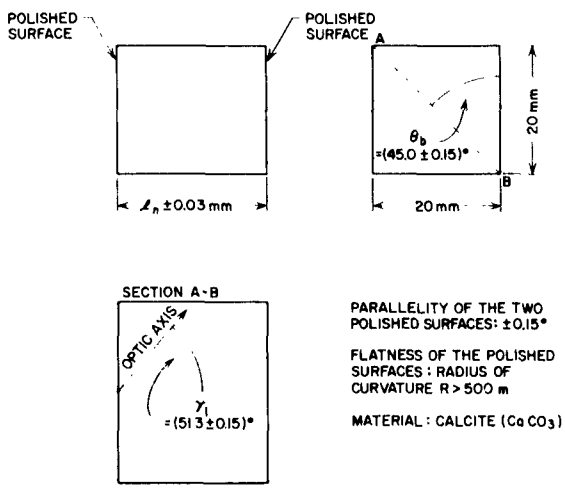

Figure 6.3. Dimensions of the birefringent crystal.

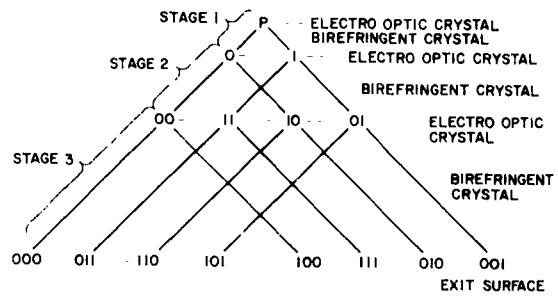

Figure 7.1. Diagram of the positions of an eight-position light deflector.

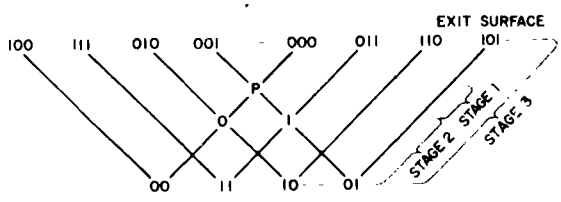

Figure 7.2. Diagram of the positions of an eight-position light deflector with the largest atage turned 180 degrees.

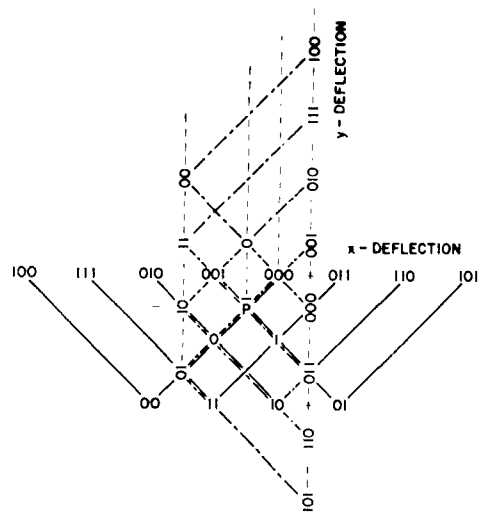

Figure 7.3. Diagram of the positions of two eight-position light deflectors.

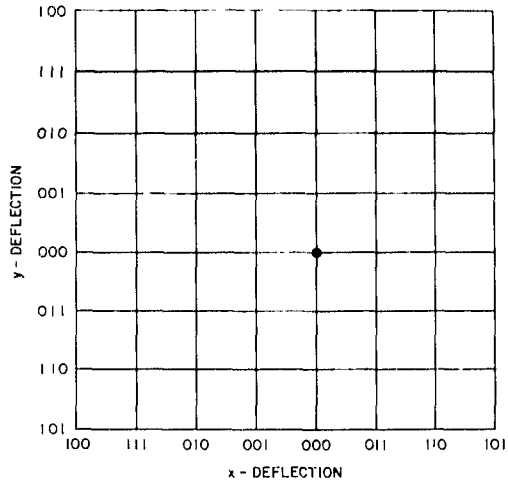

Figure 7.4. Diagram of the positions of an eight-position light deflector.

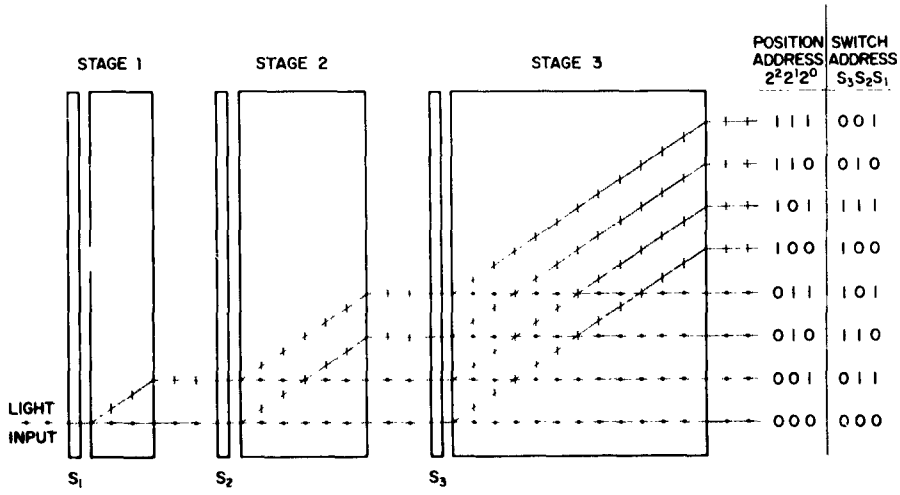

Figure 7.5. Switch addresses and position addresses.

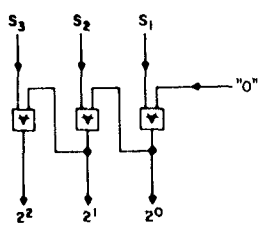

Figure 7.6. Analog circuit for converting awitch addresses to position addresses.

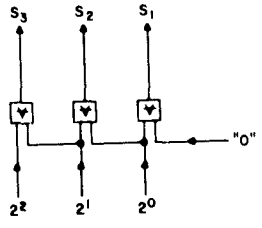

Figure 7.7. Analog circuit for converting position addresses to switch addresses.

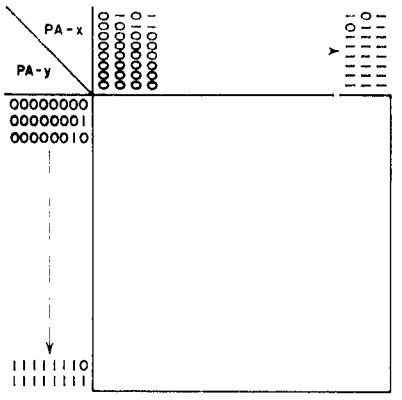

Figure 7.8. Coordinates for deflector output positions.

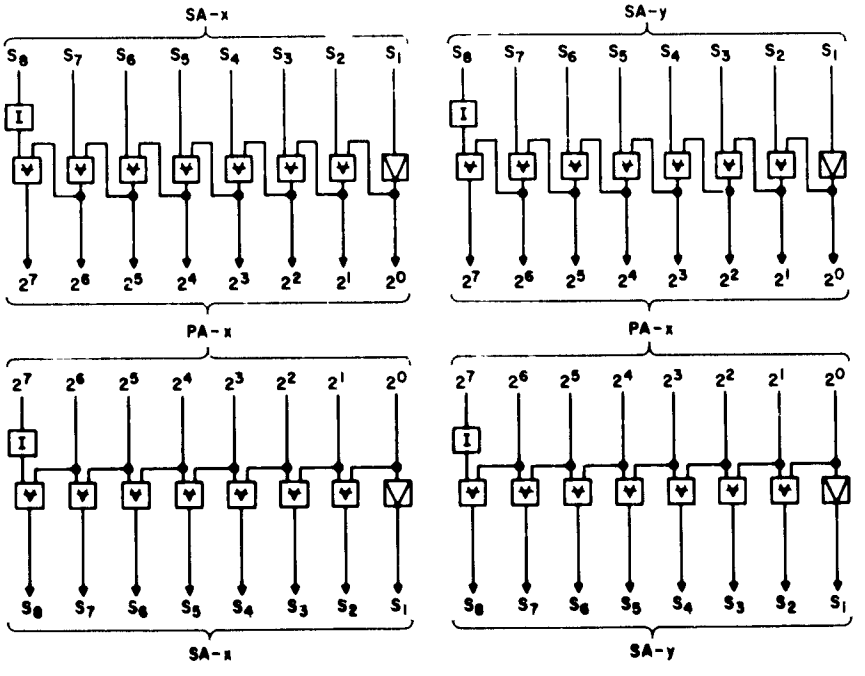

Figure 7.9. Analog circuit for an 8 x 8 stage, two-dimensional light deflector with an inverted eighth stage.

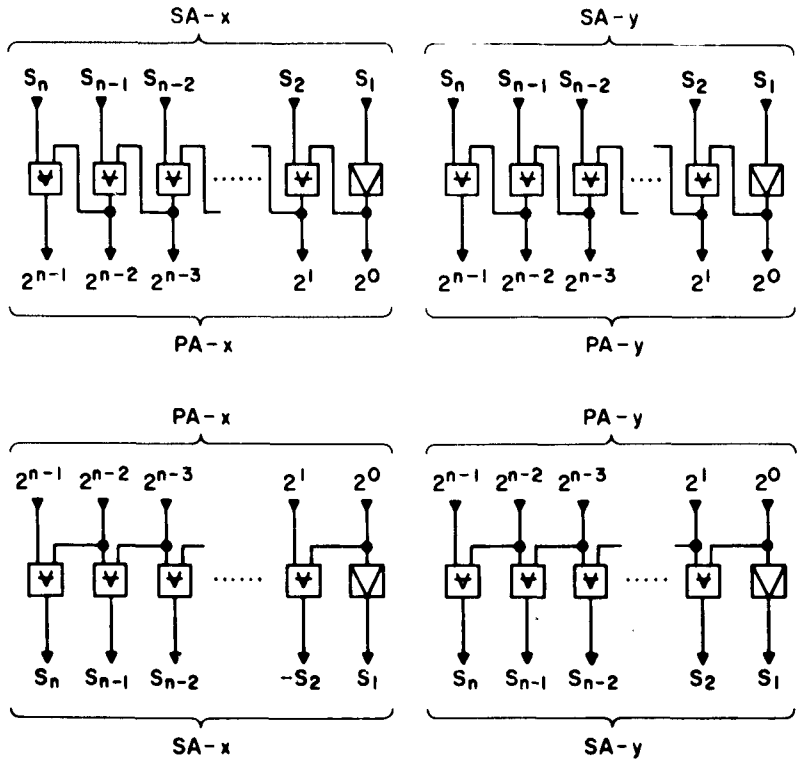

Figure 7.10. Analog circuit for two-dimensional light deflector.

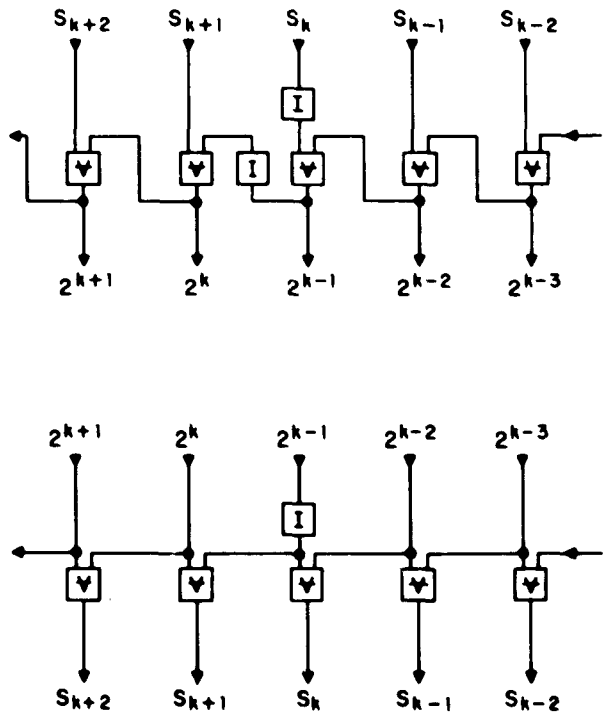

Figure 7.11. Analog circuit for n-stage light deflector with inverted k-th stage.

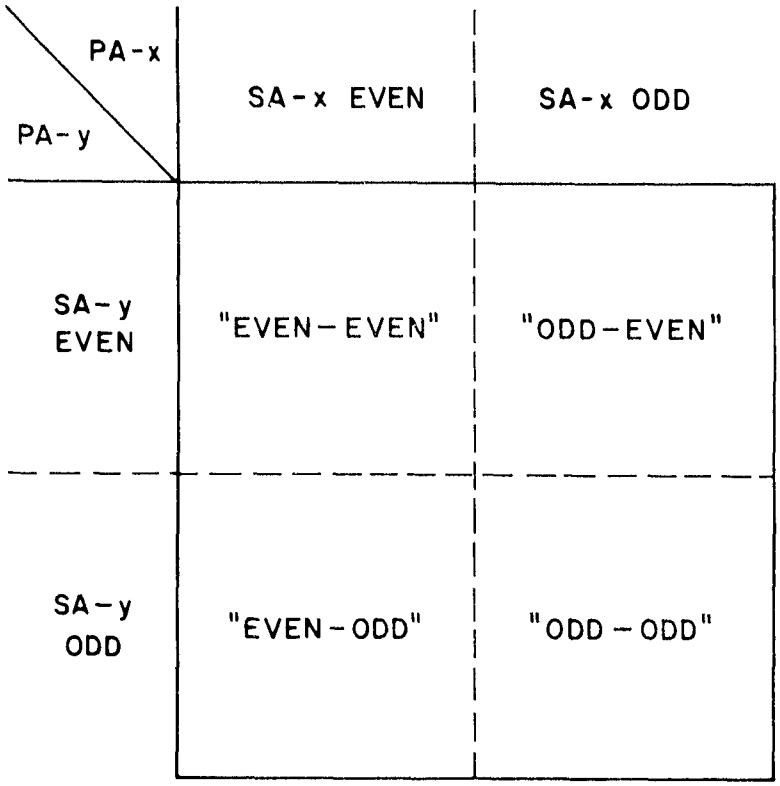

Figure 7.12. Parity quadrants of the switch addresses in the position address area.

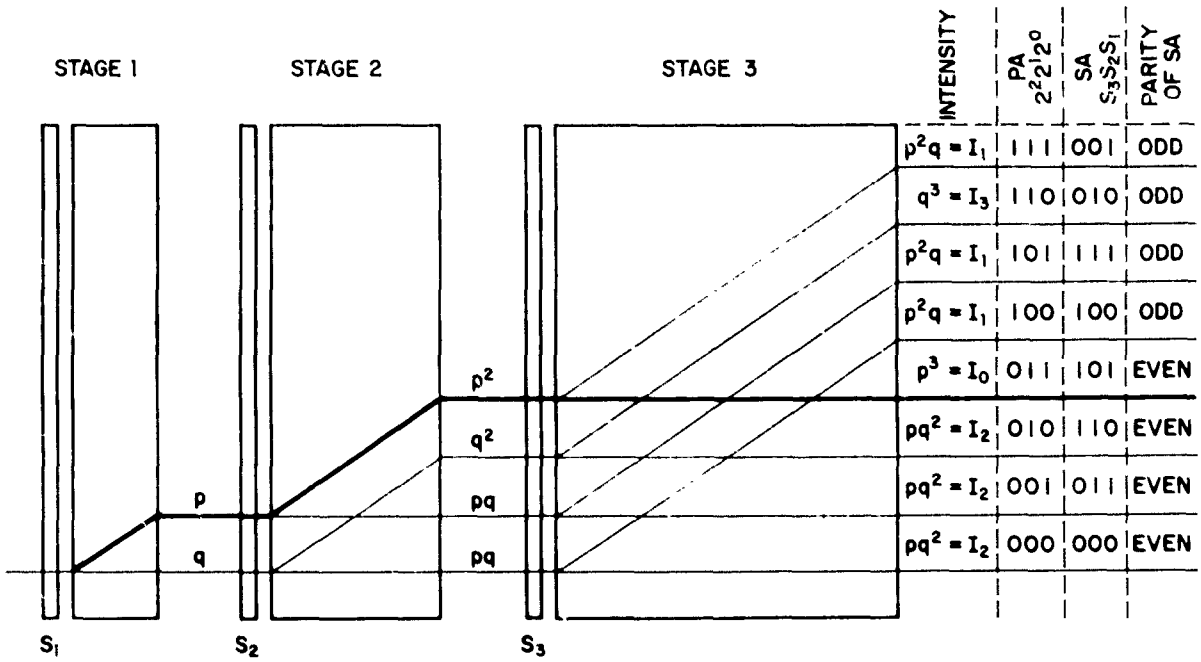

Figure 8.1. Noise distribution in a three-stage light deflector.

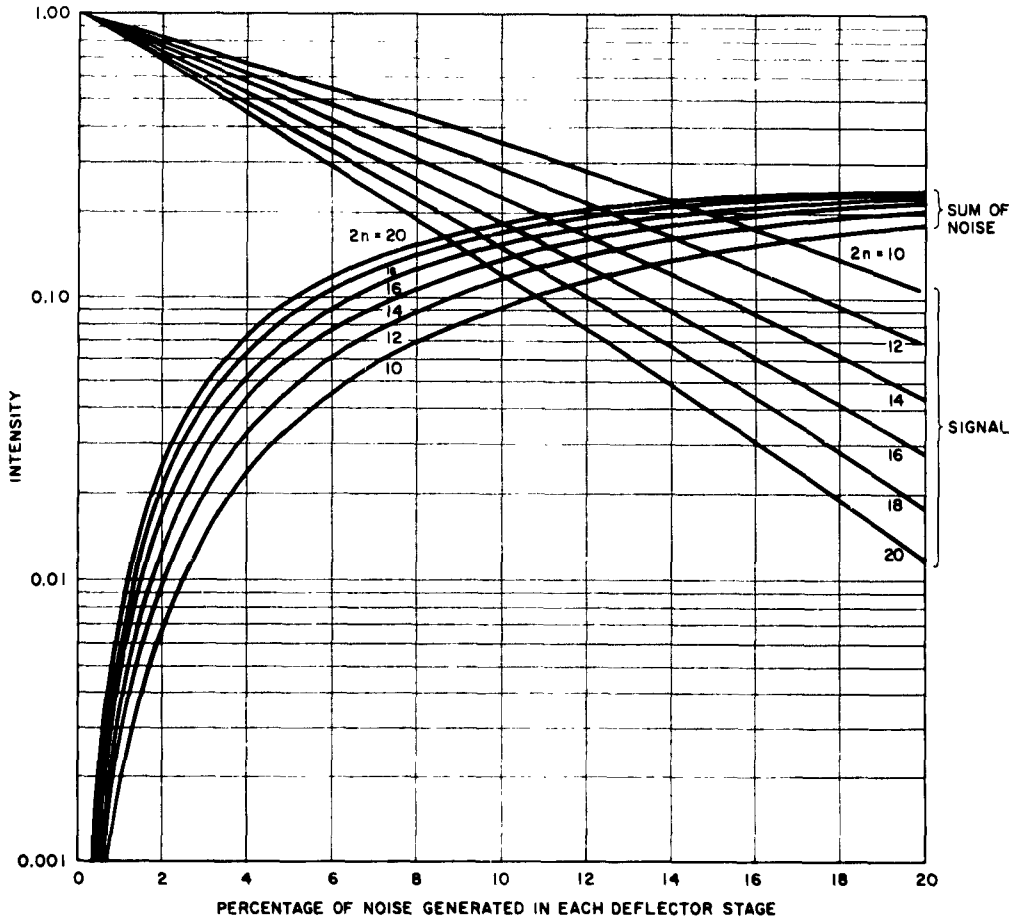

Figure 8.2. Signal and noise in the address quadrant.

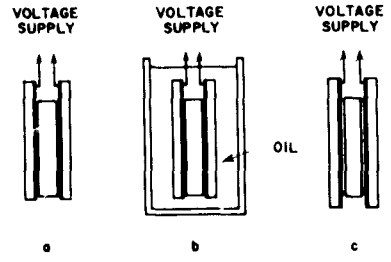

Figgure 9.1. Crystal mounting.

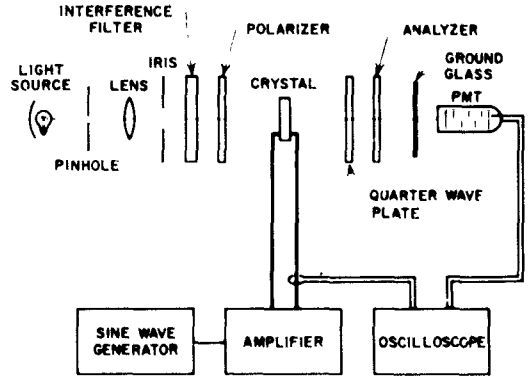

Figure 9.2. Arrangement for resonance measurements.

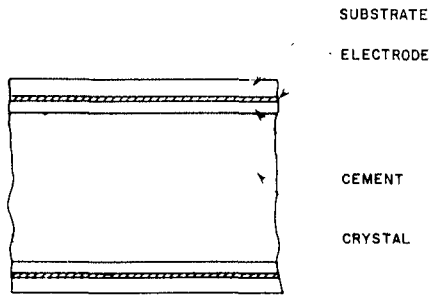

Fig. 10.1. Electrode mounting.

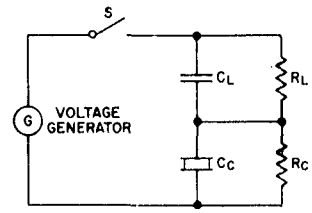

Figure 10.2. Circuit used to determine the electrical properties of the cemented electrode shown in Fig. 10.1.

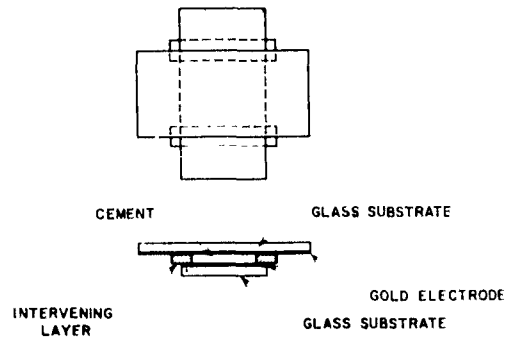

Figure 10.3. Sample arrangement for dielectric strength measurement.

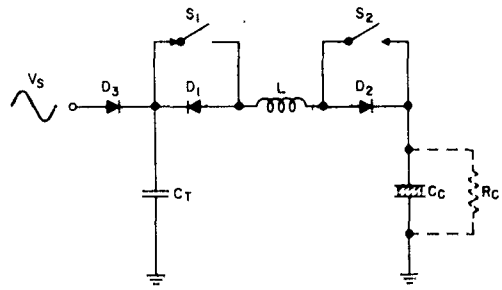

Figure 11.1. Principle of HVTTS.

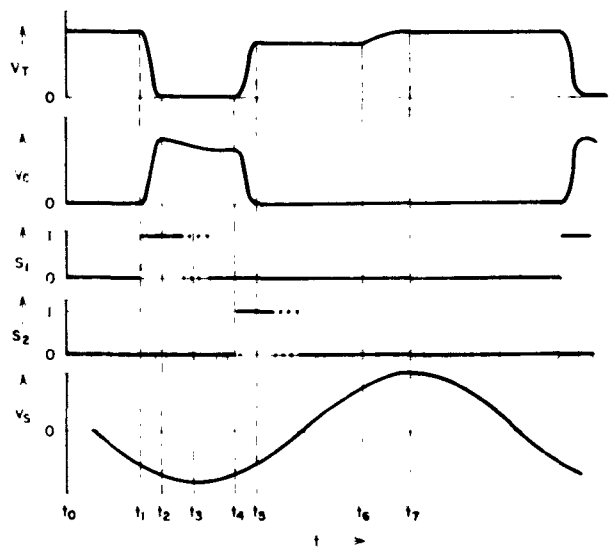

Figure 11.2. Time chart of HVTTS.

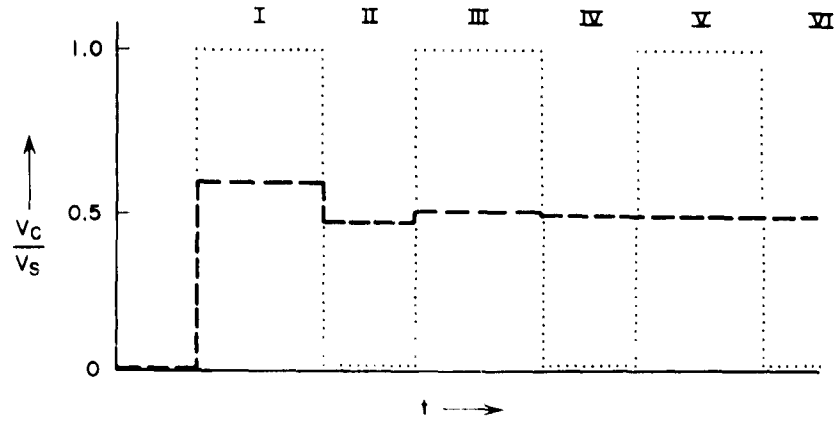

Figure 11.3. Low-speed simulation of HVTTS.
$C_T = C_C = 30\mu f$; L = 4.8h; Q = 0.4

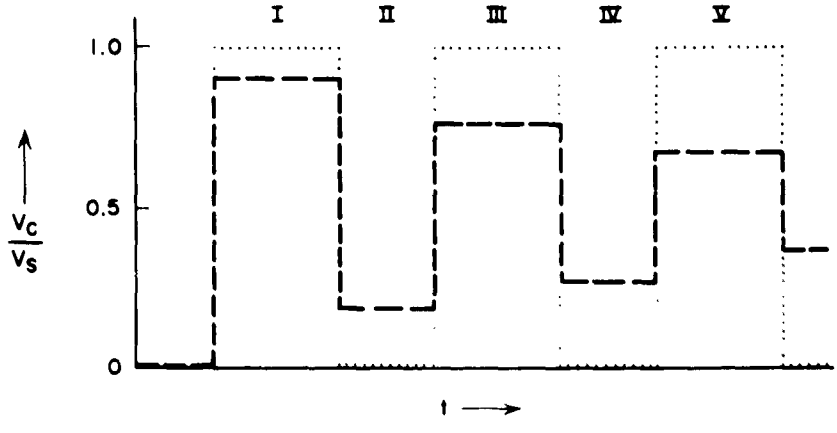

Figure 11.4. Low-speed simulation of HVTTS.
$C_T = C_C = 0.1\mu f$; L = 4.8h; Q = 7

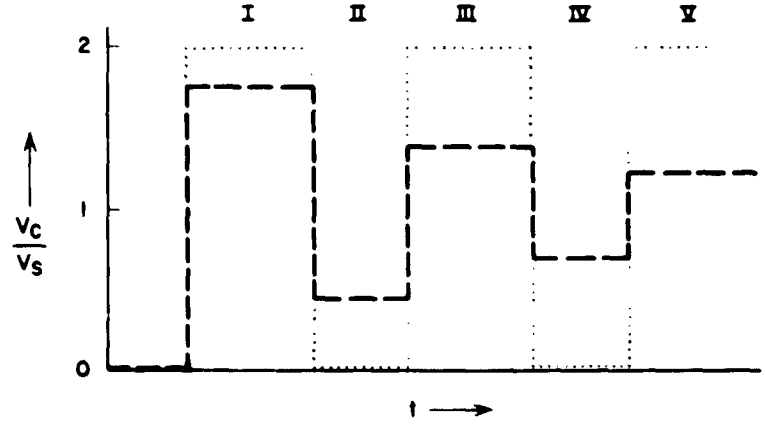

Figure 11.5. Low-speed switching of HVTTS.
$C_T = 3\ \mu f$; $C_C = 0.1\mu f$; L=4.8h; Q=5

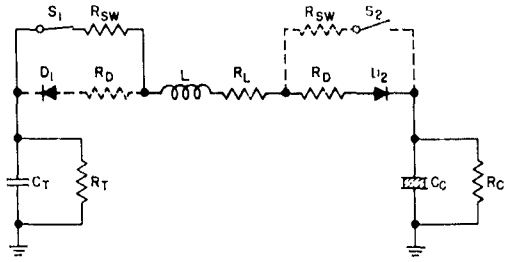

Figure 11.6. Equivalent diagram of the HVTTS including loss resistances.

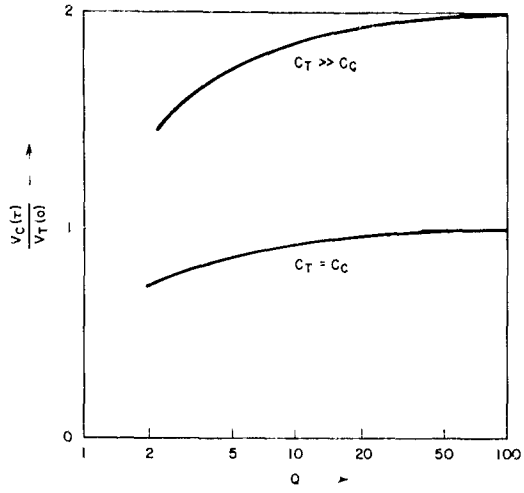

Figure 11.7. Amplitude of switching pulse in dependence on Q.

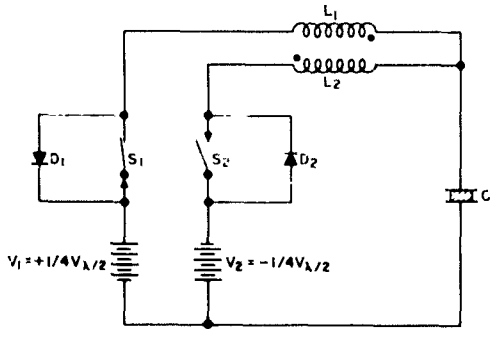

Figure 11.8. Principle of SHPMS.

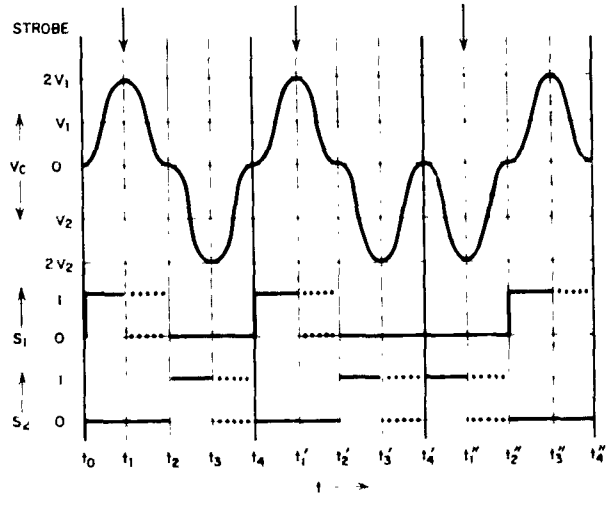

Figure 11.9. Timing Chart of SHPMS.

DISTRIBUTION LIST

	Copies
Office of the Assistant Secretary of Defense Room 3E1065, The Pentagon Washington 25, D. C.	1
Chief of Research and Development Department of the Army Washington 25, D. C.	2
Chief, U. S. Army Security Agency ATTN: ACofS, G4 (Technical Library) Arlington Hall Station Arlington 12, Virginia	2
Deputy President, U. S. Army Security Agency Board Arlington Hall Station Arlington 12, Virginia	1
Defense Intelligence Agency ATTN: DIARD Washington, D. C. 20301	1
Commanding General, U. S. Army Materiel Command ATTN: R & D Directorate Washington, D. C. 20315	2
Commanding General, U. S. Army Materiel Command ATTN: AMCRD-RS-PE Washington, D. C. 20315	1
Commanding General, U. S. Army Materiel Command ATTN: AMCRD-PE-E-C Washington, D. C. 20315	1
Commanding Officer, U. S. Army Combat Developments Command ATTN: CDCMR-E Fort Belvoir, Virginia	1
Commanding General, U. S. Army Combat Developments Command Communications-Electronics Agency Fort Huachuca, Arizona	1
Commandant U. S. Army Air Defence School ATTN: Command & Staff Dept. Fort Bliss, Texas	1
Rome Air Development Center ATTN: RAALD Griffiss Air Force Base New York	1

	Copies
Aeronautical Systems Division Wright-Patterson Air Force Base, Ohio 45433	1
Air Force Cambridge Research Laboratories ATTN: CRXL-R L. G. Hanscom Field Bedford, Massachusetts	1
Director U. S. Naval Research Laboratory ATTN: Code 2027 Washington, D. C. 20390	1
Commanding Officer & Director U. S. Navy Electronics Laboratory ATTN: Library San Diego 52, California	1
Commanding Officer U. S. Army Electronics Research & Development Activity ATTN: AMSEL-RD-WS-A White Sands, New Mexico 88002	1
Director, Monmouth Office U. S. Army Combat Developments Command Communications-Electronics Agency Fort Monmouth, New Jersey	1
Director, Materiel Readiness Directorate Hq. U. S. Army Electronics Command ATTN: AMSEL-MR Fort Monmouth, New Jersey	1
Marine Corps Liaison Office U. S. Army Electronics Laboratories ATTN: AMSEL-RD-LNR Fort Monmouth, New Jersey	1
AFSC Scientific/Technical Liaison Office U. S. Army Electronics Laboratories ATTN: AMSEL-RD-LNA Fort Monmouth, New Jersey	1
Director U. S. Army Electronics Laboratories ATTN: Logistics Division Fort Monmouth, New Jersey (MARKED FOR PROJECT ENGINEER)	8

	Copies
Director U. S. Army Electronics Laboratories ATTN: AMSEL-RD-DR Fort Monmouth, New Jersey	1
Director U. S. Army Electronics Laboratories ATTN: Technical Documents Center (AMSEL-RD-ADT) Fort Monmouth, New Jersey	1
Director U. S. Army Electronics Laboratories ATTN: AMSEL-RD-ADO-RHA Fort Monmouth, New Jersey	1
Commander Defense Documentation Center ATTN: TISIA Cameron Station, Bldg. 5 Alexandria, Virginia 22314	15
Advisory Group on Electron Devices 346 Broadway, 8th Floor New York 13, N. Y.	3
Commanding General, USASCC ATTN: SCCCD-3 - Lt. Rogers Washington, D. C. 20315	1
Office of Naval Research U. S. Naval Training Device Center ATTN: Code 53 Port Washington, New York	1
Director U. S. Army Electronics Laboratories ATTN: AMSEL-RD/P Fort Monmouth, New Jersey	1
Director U. S. Army Electronics Laboratories ATTN: AMSEL-RD/NO-4 Fort Monmouth, New Jersey	1
Commanding Officer Hq. Rome Air Development Center Research and Technology Division ATTN: RASGN/M. Kesselman Air Force Systems Command, USAF Griffiss Air Force Base, New York	1

	Copies
Dr. Selig Starr Office of Chief of Research & Development Department of the Army Washington 25, D. C.	1
Mr. Lewis R. Blair, Jr. Television & Electronic Display Division Audio Visual Comm. Directorate Office Chief Signal Officer Room 5A 466, The Pentagon Washington 25, D. C.	1
Dr. C. A. Rosen Applied Physics Laboratory Stanford Research Institute Menlo Park, California	1
Mr. Edmund F. Klein The National Cash Register Company Electronics Div., Military Dep. 2815 West El Segundo Boulevard Hawthorne, California 90250	1
Commanding General U. S. Army Air Defense Command ATTN: ADGCF Ent Air Force Base, Colorado 80912	1
Director, National Security Agency 9800 Savage Road Fort George G. Meade ATTN: R422 (J. C. Davis) Maryland	1
Scientific and Technical Information Facility ATTN: NASA Representative (SAK/DL) P. O. Box 5700 Bethesda, Maryland 20014	
Director U. S. Army Electonics Laboratories ATTN: AMSEL-RD/NP-4 Fort Monmouth, New Jersey	1
Office of the Program Manager Command Control Information System-1970 U. S. Army Materiel Command ATTN: AMCPM-CC Fort Belvoir, Virginia 220606	1

	Copies
Commanding General U. S. Army Electronics Command ATTN: Communications/ADP Commodity Office Fort Monmouth, New Jersey 07703	1
Director U. S. Army Electronics Laboratories ATTN: AMSEL-RD/PRG Fort Monmouth, New Jersey	1
Chief, Bureau of Ships Navy Department ATTN: Code 681 A-1B Washington, D. C.	1

AD UNCLASSIFIED

Development Lab., International Business Machines, Poughkeepsie, N. Y.
USE OF OPTICAL MASERS IN DISPLAYS AND PRINTERS
Quarterly Progress Report No. 5 for 24 Feb.-23 May, 64 by W. Kulcke, K. Kosanke, E. Max, & H. Fleisher, 10 Aug. 64, 66p. incl. illus, tables, 6 refs.
Contract DA-36-039-AMC-00118(E) Report Unclassified

DESCRIPTORS: (Lasers, Focusing, Conical Refraction, Digital Deflection, Display Systems, Optical Images, Input-output Devices.)

The objective is to improve electro-optic input-output devices by using the laser as an electro-optic tool. This report is concerned with further investigations into the digital electro-optic deflector. Design specs. related to aperture, spot size, spot positions, and background light (noise) are calaculated as functions of the number of deflection stages for various crystal materials. From the calculations, the specs. (over)

AD UNCLASSIFIED

Development Lab., International Business Machines, Poughkeepsie, N. Y.
USE OF OPTICAL MASERS IN DISPLAYS AND PRINTERS
Quarterly Progress Report No. 5 for 24 Feb.-23 May, 64 by W. Kulcke, K. Kosanke, E. Max, & H. Fleisher, 10 Aug. 64, 66p incl. illus, tables, 6 refs.
Contract DA-36-039-AMC-00118(E) Report Unclassified

DESCRIPTORS: (Lasers, Focusing, Conical Refraction, Digital Deflection, Display Systems, Optical Images, Input-output Devices.)

The objective is to improve electro-optic input-output devices by using the laser as an electro-optic tool. This report is concerned with further investigations into the digital electro-optic deflector. Design specs. related to aperture, spot size, spot positions, and background light (noise) are calculated as functions of the number of deflection stages for various crystal materials. From the calculations, the specs. (over)

AD UNCLASSIFIED

Development Lab., International Business Machines, Poughkeepsie, N. Y.
USE OF OPTICAL MASERS IN DISPLAYS AND PRINTERS
Quarterly Progress Report No. 5 for 24 Feb.-23 May, 64 by W. Kulcke, K. Kosanke, E. Max, & H. Fleisher, 10 Aug. 64, 66p. incl. illus, tables, 6 refs.
Contract DA-36-039-AMC-00118(E) Report Unclassified

DESCRIPTORS: (Lasers, Focusing, Conical Refraction, Digital Deflection, Display Systems, Optical Images, Input-output Devices.)

The objective is to improve electro-optic input-output devices by using the laser as an electro-optic tool. This report is concerned with further investigations into the digital electro-optic deflector. Design specs. related to aperture, spot size, spot positions, and background light (noise) are calculated as functions of the number of deflection stages for various crystal materials. From the calculations, the specs. (over)

AD UNCLASSIFIED

Development Lab., International Business Machines, Poughkeepsie, N. Y.
USE OF OPTICAL MASERS IN DISPLAYS AND PRINTERS
Quarterly Progress Report No. 5 for 24 Feb.-23 May, 64 by W. Kulcke, K. Kosanke, E. Max, & H. Fleisher, 10 Aug. 64, 66p. incl. illus, tables, 6 refs.
Contract DA-36-039-AMC-00118(E) Report Unclassified

DESCRIPTORS: (Lasers, Focusing, Conical Refraction, Digital Deflection, Display Systems, Optical Images, Input-output Devices.)

The objective is to improve electro-optic input-output devices by using the laser as an electro-optic tool. This report is concerned with further investigations into the digital electro-optic deflector. Design specs. related to aperture, spot size, spot positions, and background light (noise) are calculated as functions of the number of deflection stages for various crystal materials. From the calculations, the specs. (over)

of the birefringent and electro-optic crystals and their tolerances were evaluated for a two-dimensional deflector of 256 x 256 positions. The relation between the address of an output position and the input signal to the switches is reported; and the distribution of noise, i.e. the light intensity in unswitched positions, is described. Futher investigations refer to the frequency response & the electrode problem of the electro-optic crystals. Two electronic circuits which appear to be suited for high-speed, low-power switching of the light deflector are discussed.

of the birefringent and electro-optic crystals and their tolerances were evaluated for a two-dimensional deflector of 256 x 256 positions. The relation between the address of an output position and the input signal to the switches is reported; and the distribution of noise, i.e. the light intensity in unswitched positions, is described. Futher investigations refer to the frequency response & the electrode problem of the electro-optic crystals. Two electronic circuits which appear to be suited for high-speed, low-power switching of the light deflector are discussed.

of the birefringent and electro-optic crystals and their tolerances were evaluated for a two-dimensional deflector of 256 x 256 positions. The relation between the address of an output position and the input signal to the switches is reported; and the distribution of noise, i.e. the light intensity in unswitched positions, is described. Futher investigations refer to the frequency response and the electrode problem of the electro-optic crystals. Two electronic circuits which appear to be suited for high-speed, low-power switching of the light deflector are discussed.

of the birefringent and electro-optic crystals and their tolerances were evaluated for a two-dimensional deflector of 256 x 256 positions. The relation between the address of an output position and the input signal to the switches is reported; and the distribution of noise, i.e. the light intensity in unswitched positions, is described. Futher investigations refer to the frequency response and the electrode problem of the electro-optic crystals. Two electronic circuits which appear to be suited for high-speed, low-power switching of the light deflector are discussed.

AD UNCLASSIFIED

Development Lab., International Business Machines, Poughkeepsie, N. Y.
USE OF OPTICAL MASERS IN DISPLAYS AND PRINTERS
Quarterly Progress Report No. 5 for 24 Feb.-23 May, 64 by W. Kulcke, K. Kosanke, E. Max, & H. Fleisher, 10 Aug. 64, 66p. incl. illus, tables, 6 refs.
Contract DA-36-039-AMC-00118(E) Report Unclassified

DESCRIPTORS: (Lasers, Focusing, Conical Refraction, Digital Deflection, Display Systems, Optical Images, Input-output Devices.)

The objective is to improve electro-optic input-output devices by using the laser as an electro-optic tool. This report is concerned with further investigations into the digital electro-optic deflector. Design specs. related to aperture, spot size, spot positions, and background light (noise) are calaculated as functions of the number of deflection stages for various crystal materials. From the calculations, the specs. (over)

AD UNCLASSIFIED

Development Lab., International Business Machines, Poughkeepsie, N. Y.
USE OF OPTICAL MASERS IN DISPLAYS AND PRINTERS
Quarterly Progress Report No. 5 for 24 Feb.-23 May, 64 by W. Kulcke, K. Kosanke, E. Max, & H. Fleisher, 10 Aug. 64, 66p incl. illus, tables, 6 refs.
Contract DA-36-039-AMC-00118(E) Report Unclassified

DESCRIPTORS: (Lasers, Focusing, Conical Refraction, Digital Deflection, Display Systems, Optical Images, Input-output Devices.)

The objective is to improve electro-optic input-output devices by using the laser as an electro-optic tool. This report is concerned with further investigations into the digital electro-optic deflector. Design specs. related to aperture, spot size, spot positions, and background light (noise) are calculated as functions of the number of deflection stages for various crystal materials. From the calculations, the specs. (over)

AD UNCLASSIFIED

Development Lab., International Business Machines, Poughkeepsie, N. Y.
USE OF OPTICAL MASERS IN DISPLAYS AND PRINTERS
Quarterly Progress Report No. 5 for 24 Feb.-23 May, 64 by W. Kulcke, K. Kosanke, E. Max, & H. Fleisher, 10 Aug. 64, 66p. incl. illus, tables, 6 refs.
Contract DA-36-039-AMC-00118(E) Report Unclassified

DESCRIPTORS: (Lasers, Focusing, Conical Refraction, Digital Deflection, Display Systems, Optical Images, Input-output Devices.)

The objective is to improve electro-optic input-output devices by using the laser as an electro-optic tool. This report is concerned with further investigations into the digital electro-optic deflector. Design specs. related to aperture, spot size, spot positions, and background light (noise) are calculated as functions of the number of deflection stages for various crystal materials. From the calculations, the specs. (over)

AD UNCLASSIFIED

Development Lab., International Business Machines, Poughkeepsie, N. Y.
USE OF OPTICAL MASERS IN DISPLAYS AND PRINTERS
Quarterly Progress Report No. 5 for 24 Feb.-23 May, 64 by W. Kulcke, K. Kosanke, E. Max, & H. Fleisher, 10 Aug. 64, 66p. incl. illus, tables, 6 refs.
Contract DA-36-039-AMC-00118(E) Report Unclassified

DESCRIPTORS: (Lasers, Focusing, Conical Refraction, Digital Deflection, Display Systems, Optical Images, Input-output Devices.)

The objective is to improve electro-optic input-output devices by using the laser as an electro-optic tool. This report is concerned with further investigations into the digital electro-optic deflector. Design specs. related to aperture, spot size, spot positions, and background light (noise) are calculated as functions of the number of deflection stages for various crystal materials. From the calculations, the specs. (over)

of the birefringent and electro-optic crystals and their tolerances were evaluated for a two-dimensional deflector of 256 x 256 positions. The relation between the address of an output position and the input signal to the switches is reported; and the distribution of noise, i.e. the light intensity in unswitched positions, is described. Futher investigations refer to the frequency response & the electrode problem of the electro-optic crystals. Two electronic circuits which appear to be suited for high-speed, low-power switching of the light deflector are discussed.

of the birefringent and electro-optic crystals and their tolerances were evaluated for a two-dimensional deflector of 256 x 256 positions. The relation between the address of an output position and the input signal to the switches is reported; and the distribution of noise, i.e. the light intensity in unswitched positions, is described. Futher investigations refer to the frequency response & the electrode problem of the electro-optic crystals. Two electronic circuits which appear to be suited for high-speed, low-power switching of the light deflector are discussed.

of the birefringent and electro-optic crystals and their tolerances were evaluated for a two-dimensional deflector of 256 x 256 positions. The relation between the address of an output position and the input signal to the switches is reported; and the distribution of noise, i.e. the light intensity in unswitched positions, is described. Futher investigations refer to the frequency response and the electrode problem of the electro-optic crystals. Two electronic circuits which appear to be suited for high-speed, low-power switching of the light deflector are discussed.

of the birefringent and electro-optic crystals and their tolerances were evaluated for a two-dimensional deflector of 256 x 256 positions. The relation between the address of an output position and the input signal to the switches is reported; and the distribution of noise, i.e. the light intensity in unswitched positions, is described. Futher investigations refer to the frequency response and the electrode problem of the electro-optic crystals. Two electronic circuits which appear to be suited for high-speed, low-power switching of the light deflector are discussed.